12-2016

Nanoscale Solutions to Tailor Fiber Architectures for Realizing Composites with Triumvirate Properties

Vishnu Priya Ramineni
Clemson University

NANOSCALE SOLUTIONS TO TAILOR FIBER ARCHITECTURES FOR REALIZING COMPOSITES WITH TRIUMVIRATE PROPERTIES

A Thesis
Presented to
the Graduate School of
Clemson University

In Partial Fulfillment
of the Requirements for the Degree
Master of Science
Mechanical Engineering

---

by
Vishnu Priya Ramineni
December 2016

Accepted by:
Dr. Huijuan Zhao, Committee Chair
Dr. Srikanth Pilla, Committee Co-Chair
Dr. Gang Li

ABSTRACT

The paramount need for the development of multifunctional, smart and adaptive material systems for application in industries like automobile, aeronautical and aerospace is undeniable. Polymer composites are fast becoming the primary material options to this demand in light of their superior mechanical properties, low density, high corrosion resistance and easy manufacturability. The design flexibility offered in terms of achieving higher specific properties and light weighting is the key reason behind their success. Among all the properties that composites possess, it is the stiffness, strength and toughness that most applications mandate. These properties however, provide complimentary and contrasting characteristics for composites thereby limiting them for wide variety of applications. Hence it is critical to design composites with these triumvirate properties, which are capable of producing superior performance over their conventional counterparts.

This research aims at providing solutions to this problem by altering the constituent material architectures. '*Roding*' architecture, innovated via this study, is an integration between '*Rod*' and '*Dampening*' elements. This is an ingenious design capable of realizing the above mentioned triumvirate properties, comprising of 'Rod' elements that are capable of improving the strength and stiffness and 'Dampening' elements that can enhance the toughness. This overarching goal of realizing these triumvirate properties in a composite material system can be achieved through various methods like iterating the combinations and modifications of the nanofiller's shape, size, topology, chemical composition and even

the surface charge. In this thesis however, this concept was proven via realizing the 'Roding' architecture at a nanoscale by covalently coupling 'Rod' like single walled carbon nanotubes and 'Damper' like hyperbranched polymers. This concept can potentially be translated into micro and macro scales to suit the mass production needs of the transportation industry. The catch here is not to restrict ourselves to a particular morphology but to explore the possibilities of customizing the composite material's morphology, as per application needs.

Nanofillers with 'Roding' architecture were synthesized by optimizing the interplay between the individual nanoparticle's shape, dimension, composition and interface. Integrating the triumvirate properties of strength, stiffness and toughness into the matrix by controlling the architecture of these nanofillers is the essence of this attempt. Once nanofillers with 'Roding' structure have been successfully synthesized, they were embedded into a thermoset matrix called 'Diglycidyl ether of bisphenol-A' (DGEBA). Techniques like FTIR, Raman, XPS, XRD, TGA, Gel Fraction, ATR and FE-SEM, have been used to characterize the physical, chemical and structural aspects of the hybrid 'Roding Nanofillers'. This composite material then was also tested for its performance using standard tensile tests in order to analyze the properties of the material and the optimum loading ratios of the nanofillers. As expected the material exhibited increased strength and stiffness as well as mechanical toughness. A comprehensive study of potential applications of 'Roding' nanofillers into the more processable thermoplastic resins is presented. 'Roding' Nanofillers are but an example of the materials that can be custom made by engineering their morphology, to suit customer needs. In a gist, advanced

nanocomposites with higher order smart architectures that have the potential to exhibit triumvirate properties of strength, stiffness and toughness have been synthesized and tested for performance.

DEDICATION

To my beloved parents Ramineni Venkata Sivarama Krishna, Pusarla Sasikala and lovely sister, Ramineni Keerthi Priya. Thank you for all the sacrifices you have made for me and for your constant faith in me. Without you, this work would not have been a reality. You are my strength.

To my grandparents Pusarla Ramaiah Naidu, Pusarla Ratna Kumari & Ramineni Vidya Sagar. For their unconditional love, blessings and support. You are my inspiration.

AKNOWLEDGMENTS

I take this opportunity to sincerely thank my co-advisor Dr.Srikanth Pilla who has been a constant source of inspiration. He has played a great role in shaping my professional and personal skills. I would like to express my deep gratitude to my advisor Dr. Huijuan Zhao and for her patience and faith in me. She has always picked me up when I was down and put me back on the right path.

I thank Dr. Sreeprasad Sreenivasan for his valuable insights that helped in shaping this thesis.

I thank Dr. Joseph Lawrence, Dr. Lidia B. Rodriguez and Kimberly Ivy for their help in performing characterization techniques.

I am grateful to my friends Xiaoyan Yu, Ting Zheng for guiding me and for always being there for me. They have always taken time to patiently answer my questions and give their feedbacks whenever I needed help.

I am forever indebted to my parents, for making me into what I am today. I am grateful for my grandparents for their constant care and encouragement. I would also like to express my special thanks to my sister for understanding me and for making sure I take care of myself during all the tough times.

Finally, I would like to thank Almighty for blessing me with strength and health in order to finish this thesis.

TABLE OF CONTENTS

Page

Table of Contents (Continued) Page

LIST OF TABLES

LIST OF FIGURES

List of Figures (Continued) Page

1 INTRODUCTION

1.1 Structural Requirements of an Automotive BIW

Automakers are fast substituting conventional material options with light weight composites in order to achieve the CAFÉ 2025[1] targets of enhanced fuel efficiency and reduced greenhouse gas emissions. The two primary ways for achieving light weighting are, material substitution and architectural integration. Material substitution of automotive body structures, i.e. body-in-white (BIW), which accounts for more than 25 % of the vehicle weight using composites is one of the preeminent ways to achieve vehicle light weighting. Apart from reduction in the weight of the components, using composites as the substituting materials, adds on an additional advantage of architectural integration (uni-body BIW). In this research, BIW was considered as the target application, and nanocomposites were developed to achieve the material performance targets.

Figure 1.1 Weight distribution in automobiles

The main function of the BIW is to ensure the safety of the passengers. It is general knowledge that the shock tower, roof side rails, B-pillars and rocker panels of a BIW need to be made of a material that has high strength[1]. In case of a roll over crash[2], it is the strength of these structures that minimizes the risk of ejection and head injuries, potentially determining their survival. Steering column mounting beam, thin-wall body sections

require a material of high stiffness (bending and torsional). Bending stiffness determines the resistance of the structure towards the transverse load which is caused due to component and passenger weight, while the torsional stiffness withstands the twisting moments. Major structural elements like mid rail on the other hand, need to have high energy absorbing ability to facilitate dissipation of impact energy in case of frontal crash[1]. The three primary requirements for automotive body structures are : stiffness, strength & energy absorption[3]. In general, either a tradeoff or a combination of these three properties is required for the material. For example, a compromise between strength and stiffness is required in thin walled sections while an effective integration of both is needed for hinge pillar. Majority of sub elements located in the crush zone elements dictate the material requirement of high toughness and low stiffness. Therefore, in order to replace the conventional materials with composites, one needs to understand the exact performance requirements of each sub-part, as well as the overall requirement of the integrated body module. Though strength and stiffness can easily be achieved via existing nanocomposites, realizing all the three performance requirements through a single composite material has not yet become a reality. By tailoring the material architectures of the fillers at a nanoscale, this research shows possible ways of realizing composites, which can simultaneously achieve the targets for strength, stiffness, and crash energy absorption.

1.2 Polymer Nanocomposites

Hybrid materials or composite materials, are produced from the combination of two or more different materials such that, they display better performance properties than their individual constituents. The usage of these hybrid materials can be ascribed to the product

design flexibility they offer, which can be quantified in terms of their high specific properties. This shows that the possibility of achieving light weighting via composite material substitution is almost limitless. Out of these, notably polymer composites are fast becoming the mainstay of various industries in the light of their superior mechanical properties, low density, high corrosion resistance, and fabricability. The constituent material size in these polymer composites can vary from macro to nanoscale[4].

Polymer nanocomposites are a specialized subdivision of the polymer composite materials, as they have one or more of their components as polymer and have at least one of their constituents with nanoscale dimensions. Apart from nanohybrids that are found in nature, there are a plethora of manmade polymer nanocomposites which are commercially in use today[5]. There are many ways for tuning the properties of a polymer nanocomposite. We can either alter the morphology of the monomer molecules or building blocks that make up the composite material or vary the ratio of the components or both. Many researchers have developed these nano hybrids by combining the organic and inorganic nanomaterials to obtain required properties[6,7,8,9]. In fact, even inducing variations into the preprocessing and post-processing methods can also affect the material properties which in turn influence the performance of the product. Now that we have established the fact that the properties of the nanocomposites can be tailored, the question of their applicability remains.

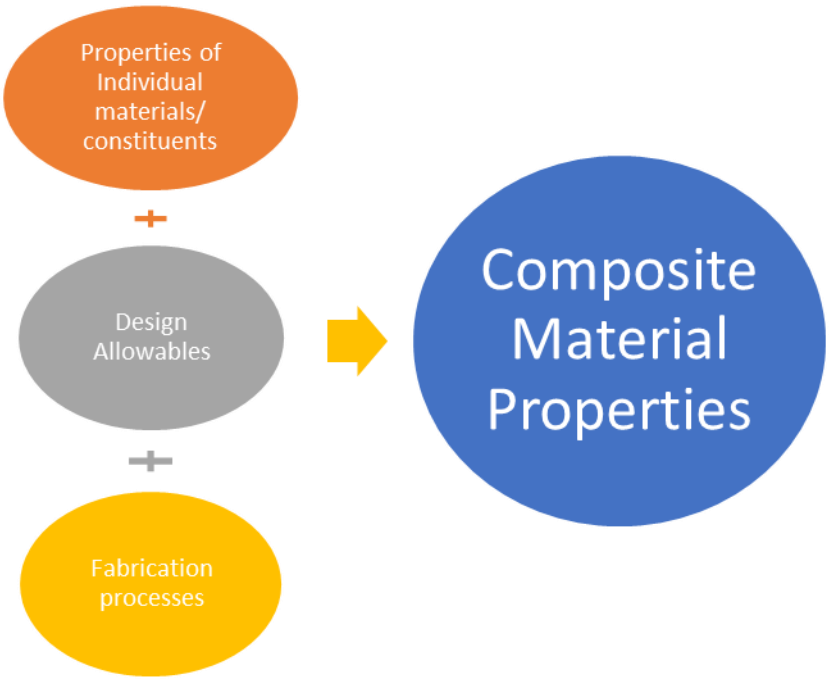

Figure 1.2 Factors controlling the properties of a composite material

1.2.1 Applications of Polymer Nanocomposites

When it comes to the applications of polymer nanocomposites, it can be confidently said that the imagination is the limit. With the modern technology, research and manufacturing abilities, almost all companies want their products to be made out of these 'new age materials'. The degree freedom of tailoring their material properties is precisely what has given them the upper hand over other conventional materials and made them the most sought out option in various industries. Here are a few of the numerous nanocomposite applications: sports goods, cables, elevators, transmission components, armor, bearings, spaceships, aircrafts, automobiles, cargo ships, flame retardant panels, LEDs, circuit boards, ceramics, structural and construction materials, wrapping films, etc. It can clearly be seen from these examples that the width and breadth of applicability of the nanocomposites cannot be denied.

1.3 Nanocomposites in Automotive Industry

GMC, Chevrolet, BMW, Mitsubishi[10],Toyota are but a few of the automobile giants that have been implementing nanotechnology in their cars for the past couple of decades. The reason behind the majority of the OEMs drifting their materials from metals and conventional plastics to nanocomposites is their high specific properties like strength, stiffness and high toughness. Increased dent/scratch/wear resistance, soil repellent nature, improved barrier properties (smoke and fire retardant), high modulus, easy to paint, better aesthetic appearance, recyclability, amplified electrical and thermal conductivity, light weight are only a few of many advantages offered by nanocomposites, that are driving this drift.

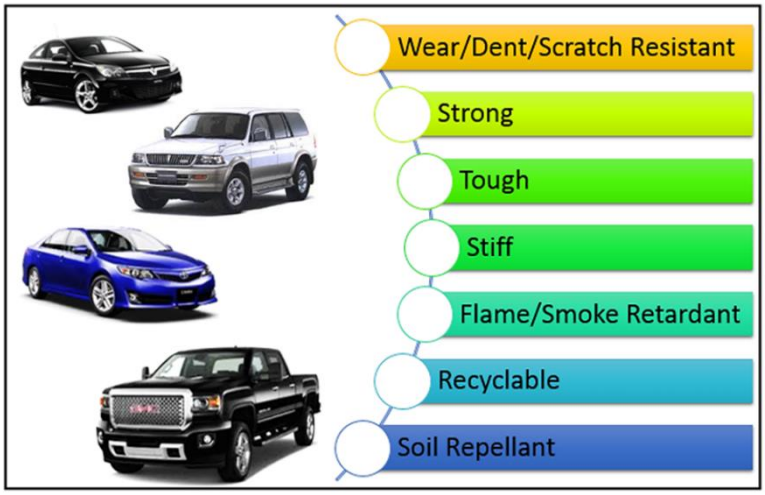

Figure 1.3 Multi-functionalities of automotive nanocomposites

Nanocomposites are being used to make a number of automobile components and this number keeps increasing day by day. Head lamp covers, tires, fuel lines, bumpers, hoods, window panels, engine covers, transmission components, outer coatings, LEDs, circuit boards, step assistants, side trims, door interiors, fuel hoses , running boards, fuel

tanks, trimming belt covers, interiors are some of many automotive components that make use of nanocomposites.

1.4 Pros and Cons of Nanocomposites

The main advantage of using polymer nanocomposites as materials for manufacturing products is the flexibility that they offer in terms of their properties. Tailoring of material properties requires extensive knowledge about which aspects of material morphology and the possible variations that can be potentially be induced into the material properties. Nanocomposites are mostly developed by incorporating nanofillers into macro and micro matrix materials. The properties of the nanohybrids mainly depend upon the following factors:

a) Nanofiller composition

b) Matrix composition

c) Nanofiller-Matrix ratio

d) Nanofiller-Matrix compatibility

e) Methods used for incorporating nanofillers into the matrix

This requires high level theoretical, experimental and computational knowledge. Material scientists are working on gathering the theoretical and modelling knowledge to produce risk-free composite materials that can be applied to products produced via mass production.

Along with the advantages of nanocomposites, come the challenges they offer. Achieving uniform dispersions between two different sizes of materials like nanofillers and macro matrices is in itself a tedious task. This can be attributed to two main reasons: high aspect ratio of the nanofillers and the lack of interactions between the nanofillers and matrices into which they are incorporated. There are multiple methods being applied to overcome this problem like surface modifications, efficient dispersion machinery, controlled working environments, chemical and physical modifications of the fillers (surfactants) & matrices and smart choice of compatible materials. Scalability, repeatability, durability, manufacturability, chemical and thermal instability, environmental stability, lead time and most importantly affordability are some of the other prime challenges associated with the applicability of nanocomposites at an industrial scale.

Ability to actually mold and engineer the morphology of the constituent materials, so that the final product is capable of reflecting the exact performance of its constituent nanocomposite material is another challenging task. This can be achieved only through experience and iterative validation of the performance of the product's components that are made with these tailored materials. Developing better and efficient manufacturing techniques and machinery capable of handling nanocomposites is one more of an uphill task that still needs to be accomplished. This can of course only grow hand in hand with emerging research on nanocomposites.

1.5 Motivation

As mentioned above, many subparts of automobile BIW need either a combination or a compromise between the structural requirements of strength, stiffness and toughness.

These requirements need to be understood from a molecular level (as we are looking at material substitution via polymer nanocomposites), in order to come up with efficient material alternatives. Mechanical stiffness of the polymer is defined as the resistance offered to the mobility of molecular chains. Introduction of reinforcements into the polymer matrix restricts the motion of polymer chains, resulting in enhancement in mechanical stiffness. Though increase in stiffness is beneficial, it should be kept in mind that the toughness keeps on decreasing with this increase. The reason for this being the fact that, the molecular chains of the polymer need to move, to be able to absorb the impact energy. Majority of the conventional nanofillers can enhance either stiffness or toughness, but not both. However, to be used as a structural material for automotive BIW application, a material needs to be strong, torsionally stiff and also have the capacity to absorb impact energy. There is no existing nanocomposite that can effectively bring together the triumvirate properties of strength, stiffness, and toughness, to the required levels. Thus, there is urgent to develop materials that can enhance these triumvirate properties in order to satisfy the requirement of multifunctional material attributes of BIW components. To capitalize on this opportunity the research hypothesis given in later section has been developed.

1.6 Research Hypothesis

I hypothesize that "A strength and stiffness enhancing 'Rod' element when covalently coupled with a toughness enhancing 'Dampening' element results in a hybrid reinforcement architecture, that when impregnated in a polymeric matrix will improve the triumvirate properties of strength, stiffness & toughness!"

Though there is a plethora of research available on material architecture modifications via physical bonding (pi-pi stacking, ionic bonding, hydrogen bonding, van Der Waals iterations, surfactants, aromatic absorption, surface adsorption, polymer wrapping), attempts to modify the structure of nanofillers via covalent bonding are comparatively scarce. This is due to the fact that covalently modifying the material morphology at a nanoscale is challenging and requires highly controlled experimentation. This thesis is an attempt to create a hybrid nanofiller with a predefined morphology (which in turn helps in achieving predefined requirements) by covalently bonding two different nanoparticles with tailored surface architectures. This has been done to better understand the influence of nanofiller morphologies on the degree of translation of the hybrid filler properties from nano to macroscale. All this has been done while keeping in mind the available manufacturing capabilities of OEMs, in order to practically correlate the obtained results with the probability of mass production.

1.7 Intellectual Merit: 'Roding' Architecture

The distinguishing feature of nanocomposite materials is the ease with which material properties can be tailored to suit specific applications. This requires applicants to have a basic understanding of the potential sources of variability introduced by utilizing composite materials. Controlling the morphology of the composite system plays a critical role in achieving the desired material performance. Thus, a new material architecture called 'Roding' that has the potential to satisfy/enhance the properties like strength, stiffness and toughness simultaneously is proposed. This architecture can be achieved at both matrix and filler levels. However, this study focused on realizing 'Roding' architecture via fillers.

Nanomaterials possess variety of morphologies or shapes such as nanospheres, nanotubes, nanofibers, nanoboxes, nanoclusters, nanoreefs, platelets, etc. Each of these morphologies has specific purpose that they help to serve (detailed literature search is present in further sections). For this initial attempt, 'Rod' like fibers/tubes that have the morphology similar to a rod element and possess high strength and elastic modulus are considered. Although fibers at various scales may be considered to test the research hypothesis, the most challenging length scale i.e. nanoscale is the focus of this research. Here carbon nanotubes are considered as 'Rod' like nanofillers since they not only have higher reinforcing efficiency but also serve plethora of additional purposes (discussed in the next section). Design of composite materials with enhanced toughening is even more complex and challenging. Toughening can be induced by numerous methods like copolymerization[11], blending with tough polymers and plasticization. These methods are often a long and costly, making them less viable options when considering large scale applications. Incorporating special additives is a facile means to enhance the toughness both from property and economic points of view. All of these options aim at varying the morphology of the composite by adding an additional element, termed dampening element, which has the capability to absorb impact energy. This 'Dampening' element plays an important role in enhancing the toughness of the composite. Hyperbranched polymers as a plausible option at nanoscale to significantly increase toughness at relatively low loading level because of their unique highly branched morphology that have the capacity to absorb energy. The branched architecture of the arms of the hyper branched polymer enables it to

stretch and contract and thus allowing it to absorb energy unlike linear polymers (which are relatively stiff and have less interfacial bonds).

The main reason that hinders the translation of extraordinary properties of the filler to matrix is the interfacial gap between the nanofiller and the matrix, there are relatively very large interfacial gaps between the matrix and filler, especially when nanoscale fillers are embedded into macroscale matrices. Particularly in CNT nanocomposites, this is even more prominent. Because the load is not effectively transferred from the matrix to the nanotubes their extraordinary properties like high strength and stiffness, cannot translate to whole of the composite material. This problem is overcome by using hybrid nanofillers with 'Roding' architecture. The HBP has a large web-like structure with extended arms, which act as compatibilizer between nanotubes and polymer matrix. The chemistry of HBP is intelligently selected, such that the end functional groups present on the arms of the HBP have the capacity to cure the epoxy. Thus, when 'Roding' nanofiller is used, one end of HBP arm is bonded to the CNT while the other end is covalently linked to the matrix. This not only leads to better adhesion but also permits effective load transfer between the matrix and the fillers due to enhanced mechanical interlocking. And because of the amorphous shape of the 'Roding' nanofillers they have the ability to embed easily into the matrix, in comparison with the crystalline rod-like pristine CNTs, that exist in agglomerates.

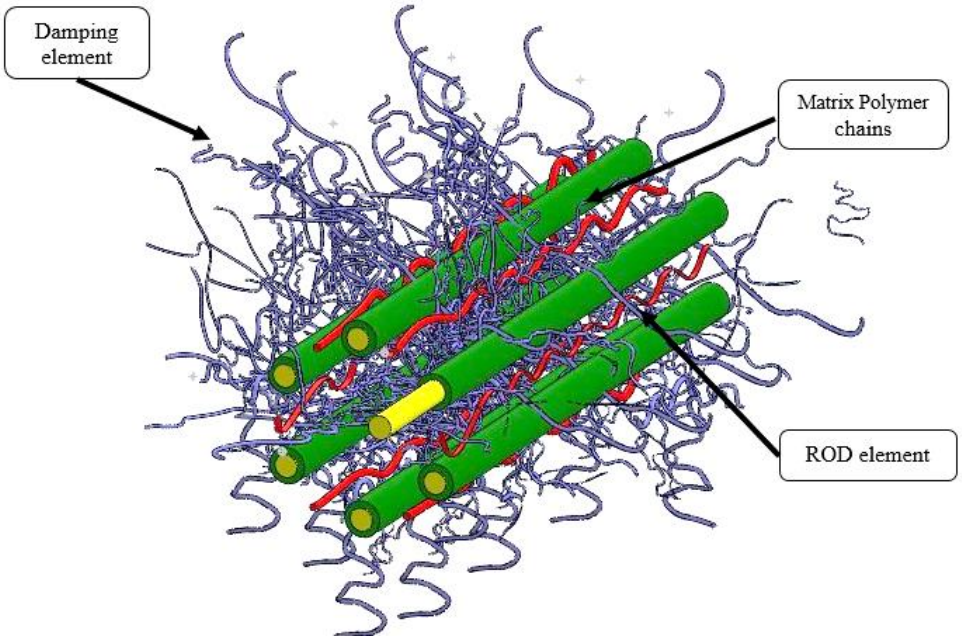

Figure 1.4 Roding architecture concept visualization

Thus, integration of the three main structural material requirements (namely toughness, stiffness, and toughness) into the nanocomposite material via controlling the architecture of 'Roding' nanofillers is the main focus of this research. This has been achieved by essentially studying how the material architecture of filler can be modified before they are introduced into a matrix. Additionally ways to improve the filler-matrix interactions via covalent bonding is also researched.

1.8 Material Options:

Nanofillers can be inorganic lipids, polymers[12-14], dendrimers, liposomes, ferritin, hydrogels, micelles, layered biopolymers, n-halamine compounds, cationic quaternary polyelectrolytes, layered biopolymers[15],etc. constitute organic nanoparticles. They can be

manufactured using wet chemical techniques, self-assembly, solvent shifting to name a few.

Nanofillers with shapes like nanotubes, nanowires and nanoplates are some of the favorites for creating nanocomposites due to various reasons like their versatile shape, easy flexibility of functional moieties, easy manufacturability (using methods like solution casting/ solvent induced intercalation, melt compounding/processing and in-situ polymerization), affordability and widespread raw material availability. One of the most notable advantages is that lower loading level of the fillers display drastic increase in properties when nanofillers are used, in comparison with conventional fillers of either macro or micro scale.

Different types of nanomaterials like carbon derived nanomaterials, inorganic nanomaterials, metallic nanomaterials and polymeric materials have the potential to act as the stiffness and strength giving 'Rod' element.

Gold nanorods[16], metallic nanorods, ZnO[17], carbon nanorods[18] , branched TiO2 nanorods[19],carbon nanotubes[20] are a few of many 'Rod' like element options for realizing 'Roding' material architecture. These rod elements can be again of various shapes and size namely solid, hollow, have cylindrical, triangular cross-sections etc.

Hairy nanoparticles, hydrogels, cellulose nanofibrils, dendrimers, hyperbranched polymers, star shaped polymers, comb polymers, dendrons, polymers, macromolecules with randomly branched carbon skeleton, etc. are among the options for 'Dampening' element.

Out of all the material options listed above, carbon nanotubes were chosen as the 'Rod' element and HBP was chosen as the 'Dampening' element in this research. The reasons for selection of these particular materials are dealt in depth in the succeeding sections along with a brief description of subdivisions among them.

1.8.1 Carbon Nanotubes

Discovery of CNT can be regarded as one of the ground shattering scientific breakthrough of the century. They are aptly called 'ultimate nanofillers' as because of their extraordinary properties listed in table. CNTs are used in numerous applications like data storage devices, structural applications, solar cells, memory devices, conductive composites, biosensors, drug delivery, fuel cells, super capacitors, conductive plastics, field emitters[21] and many more.

All carbon atoms in carbon nanotubes are in sp^2 hybridized state. They are cylindrical tubes that are formed when a single layer of graphene which is an atom thick is rolled to form a tube. The types of carbon nanotubes are listed below:

a) Single walled Carbon Nanotubes
b) Double walled Carbon Nanotubes
c) Multi walled Carbon Nanotubes
d) Coiled Carbon Nanotubes

CNTs have extraordinary mechanical properties, tensile strength more than 50 GPa and it is very difficult to break them by stretching and bending. Electrical properties of CNTs mainly depend upon their chirality, helicity, and diameter[22-24]. The elastic modulus

of SWCNTs is approximately 1 TPa[25] [26]. When materials like carbon black are used, the companies generally compromise on the color of the component. But that is not the case for components made out of CNTs. This is because CNTs are capable of increasing the conductivity of components without compromising on the color.

1.8.1.1 Single walled Carbon Nanotubes

Decisive advantages offered by CNTs like their strength, stiffness, modulus is what has compelled their selection as the 'Rod element'. Single walled carbon nanotubes/SWCNTs are formed when a single layer of graphene is seamlessly rolled up to form a tube[27]. Carbon nanotubes which have one or more carbon nanotubes of lesser diameter inside them are called multiwalled carbon nanotubes/MWCNTs. Though MWCNTs are cheaper in terms of cost than SWCNTs, they have not been chosen in this research due to reasons disused below.

Strength and stiffness of MWCNTs are just a few of the many properties in which 'SWCNTs' have an upper hand. This may be the result of less intense van der Waals interaction between layers of multi-walled nanotubes. And also because of varied range of nanotubes in a particular amount of sample, calculating young's modulus can be a bit arduous (especially in uniaxial tensile load applications) [28], mainly because these values are more dependent on the conditions and orientation of the nanotube layers. Studying these effects on the mechanical properties, aids us in better understanding exactly how MWCNTs can be comparatively less efficient in handling the transferred loads from the matrix[29].It has been proved via computational simulations that there is, in fact, slipping between the inner and outermost layers of the MWCNTs which impedes the load transfer

process[28, 30]. These challenges can, however, are avoided when SWCNTs are considered as the 'Rod' element.

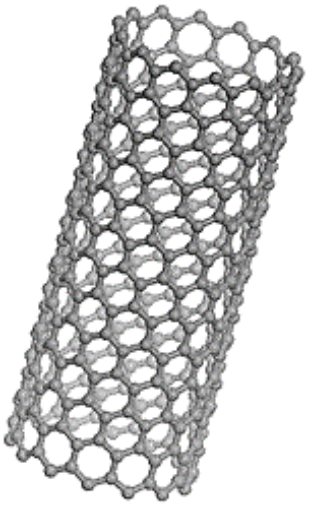

Figure 1.5 Single walled carbon nanotube

An important problem that pops up when one considers using CNTs on large scale, i.e. the achievement of their homogeneous dispersion in a composite matrix. In traditional carbon fibers, surface treatments are always used to improve interfacial bonding. The two principal ways of improving adhesion and shear strength are: increase the surface roughness, increase the surface reactivity.

Challenge	Solution
Nanofiller dispersion	Surface treatment(proper surfactants/polymers/coupling agents) Effective stirring
Interfacial nanofiller – Polymer interaction	Chemical covalent bonding between the nanofillers and the hosting polymer matrix.

Table 1-1 Solutions to overcome challenges of nanofiller dispersion

1.8.1.2 Limitations associated with the use of CNTs

Even though the properties of Carbon Nanotubes are inimitable, their wide spread commercial use is limited due to their high cost. However, the life of this disadvantage is limited. The cost of CNTs is expected to reduce in the next couple of decades, as it is predicted that the manufacturing cost of CNTs will automatically decrease with increase in their demand for large scale applications.

1.8.2 Hyperbranched Polymers

Hyperbranched polymers are one of the few nano-polymers that are widely appreciated through the domains of material science. Apart from increasing toughness hyperbranched polymer has an additional advantage of flexible functional moieties. These functional groups present at the end of the hyperbranched polymer arms can be tailored according to the chemical reactivity and affinity of the 'Rod' element and 'Matrix' simultaneously.

Hyperbranched polymers (HBPs) are multi-functional polymers that have uniquely attractive features, such as their high degree of branching (which makes them less viscous than their linear analogues with a similar molecular weight) and high reactivity (given their elevated concentration of surface groups that can be modified in order to fine-tune their physical/chemical compatibility with other polymers, substrates or resins). The numerous functional groups from HBPs facilitate a broad range of possibilities for further functionalization reactions. By controlling the number of these functional groups and their chemistry, one can competently tailor the properties like viscosity, solubility, thermal

stability, chemical reactivity, polymer miscibility and glass transition temperature of the HBP.

The introduction of multiple functional groups is achievable by coupling with groups present on the CNTs, thereby reducing the destruction of the CNTs by inevitable chemical modification or high shear dispersion. The large number of functional groups and the branched topology of HBPs effectively avoids their aggregation by their reducing the solution viscosity and degree of crystallization.

Monomers of the type AB_x (where x>=2) combine to form hyperbranched polymers. There are mainly two differences between dendrimers and hyperbranched polymers. The first difference is the shape. Dendrimers have a structured and predictable globular shape while hyperbranched polymers have a much random shape that can sometimes change upon expanding or swelling[31]. The hyperbranched polymers considered in this research are of pseudo third generation. This means that apart from completely reacted linear units in the inner layers of the branched polymers, there are many unreacted linear units present. These, in fact, can potentially influence the randomness of the structure.

1.8.3 Thermoset Matrices

Epoxy resins are the matrix materials of high interest for mass production owing to their high modulus, low shrinkage in cure, high adhesion, good chemical and corrosion resistance. Combining the properties of epoxy with CNTs can supply more extensive applications. Epoxy resin is inherently brittle, owning to the crosslinked structure of its molecules (which restricts their mobility). This brittle nature results in low resistance to

crack initiation and growth, however, this problem can be mitigated by the incorporation of nanoadditives[32,33]. Despite many achievements in the development of novel nanoadditives for epoxy, challenges still exist in materials selection to fulfill the potential of nanocomposites for large scale industrial applications.

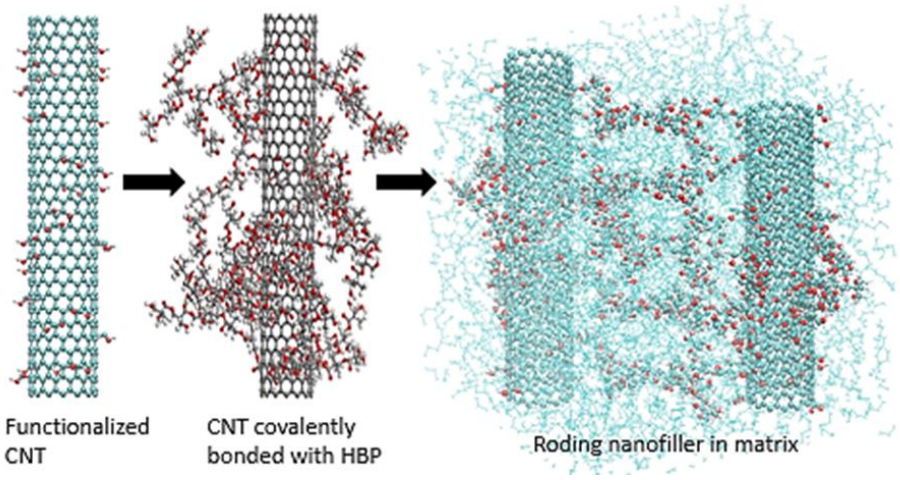

Figure 1.6 Chemical scheme used to make 'Roding' nanofillers

1.9 Organization of the Thesis

The main steps in designing composite materials with new morphologies are: decide the application, finalize the application requirement categories, modify the morphology, list different available and potential compositions to realize the hybrid morphologies, perform testing to confirm the success of the material morphology.

First, an application that has a huge impact on the world economy as well as everyday lives of people is chosen namely, automotive body structures (BIW). The three main categories of structural requirements for automotive BIW (namely stiffness, strength, and energy absorption/toughness) were presented in detail in the introduction. Available composite options and state of art of nanocomposites in automotive industry is then

presented. The motion behind the thesis is then explained in great detail along with research hypothesis. After which 'Roding' concept was introduced and plausible morphologies were mentioned, following which the reasons for selection of particular 'Rod' and 'Dampening' materials were discussed. All of the background study that led to the development of 'Roding' architecture is presented in Chapter 2, titled 'Literature search'. The Chapter 3 represents the 'Experimental section' that deals with the specifications of the materials and equipment used for this study. This is followed by a detailed explanation of the chemical schemes used to realize 'Roding' nanofillers by covalently coupling CNTs and HBP.

In order to perceive the effectiveness of filler morphology alterations, structural, chemical, thermal and optical tests were performed on the 'Roding' nanofiller. Their results and discussions of these tests are presented in Chapter 4 named 'Results and Discussion'. The conclusion obtained from these techniques, future scope of this research as well as its potential impact, are discussed in detail in Chapter 5 titled 'Conclusions and Future work'.

2 LITERATURE REVIEW

2.1 Morphology of Nanofillers

Each of the nanoparticles has a different shape, size and composition. This variation in shape is one of the key factors that impart different properties to the nanoparticles, besides composition and size. When one decides on one material scale, be in nanoscale or microscale or macroscale, he/she has the independence to manipulate the composition and particle size for tailoring the required material properties.

There is virtually no limit to the achievable variations in shape of nanoparticles. Even in their natural state they have multitude of different shapes and this number only keeps on increasing as researchers play around with their morphologies, in an attempt to tune their properties. Nanoparticle architectures can be built right from molecular level (even at atom level in some cases) in order to bring out novel and unexplored mechanical, chemical, electrical, thermal properties which can in turn be tuned and applied into next generation applications. The main reason why the material science community is more fixated on 'Nano'-level material research is due to the fact the when materials that range from 10^{-9} to 10^{-7} m (1 to 100 nm), their properties are completely different than those of their counterparts at macroscale. This is due to different factors that come into play like quantum wave-like transport, size confinement, and predominance of interfacial phenomena[34]. In order to alter the shape and morphology we need to first understand how the shape of nanomaterials effects their properties. Subsequently, we need to perform multiple iterative experiments and characterizations on the existing as well as manmade materials.

Various aspects of nanoparticle morphology like composition, size, shape, ratio of dimensions (like aspect ratio) and spherical nature can be controlled to tune the properties.

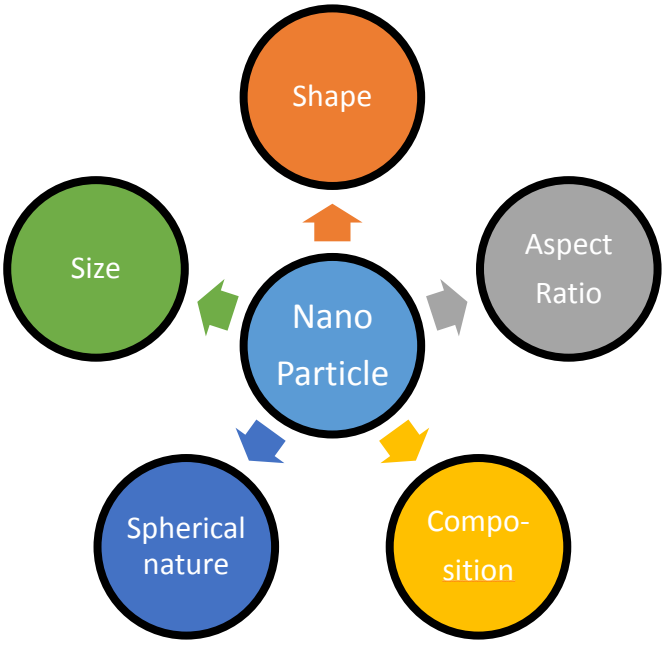

Figure 2.1 Aspects of nanoparticle morphology

The above represented five main aspects of particle morphology have been discussed in the following section, along with a few examples where, researchers have successfully modified the shape and achieved better material performance.

2.1.1 Variation in Size of the Nanoparticle

Nanoparticles that are 'long', generally exhibit high stiffness, strength and excellent electrical and thermal properties. These long nanoparticles are mostly crystalline in nature.

Here are a few examples of how the architecture of the nanoparticles was modified to obtain better properties. Mechanical strength of polycrystalline materials is largely dependent on the grain sizes given by Hall-Petch relationship shown below[34]. This law states that the material strength is inversely proportional to particle size:

$$\sigma = kd^{-1/2} + \sigma_0$$

Where

σ = Mechanical Strength

d = Grain Size

$\sigma 0$ = Shear stress in a mono-crystal required for gliding dislocations.

This conventional description of yielding that can be applied to materials at macroscale is no longer valid[35]when the material scale is reduced to nanoscale where inverse Hall-Petch effect is observed[36]. Due to change in deformation mechanisms for materials at nanoscale, the properties they exhibit can vary drastically, for example when ceramics have nano-grains of less than 50 nm, they act as super plastic materials than can deform even at application of very low loads and heat[37]. Besides mechanical properties , optical, electronic and even chemical properties are bound to change when material is compared at macro and nanoscale because the surface and composition of the nanoparticles is completely different than its macro counterpart[38].

Another example of how materials exhibit unexpected properties can be seen in[39] where the drawn composites comprising of Ag or Nb fibers embedded in a Cu matrix exhibit deviation from brittle mature(a common feature of BCC materials at macroscale) and exhibited ductility before fracture and displayed mechanical strain of 10 along with tensile strength up to 2GPa. Surface films, strands, fibers are but a few types of nanomaterial that are available in the market.

Based upon their size in different *dimensions*, nanomaterials are classified into various categories of nanostructures namely: Zero, One, Two and Three dimensional nanomaterials[40,41]. These materials are created by varying the modulation dimensionalities at nanoscale. Their graphical representation is shown below.

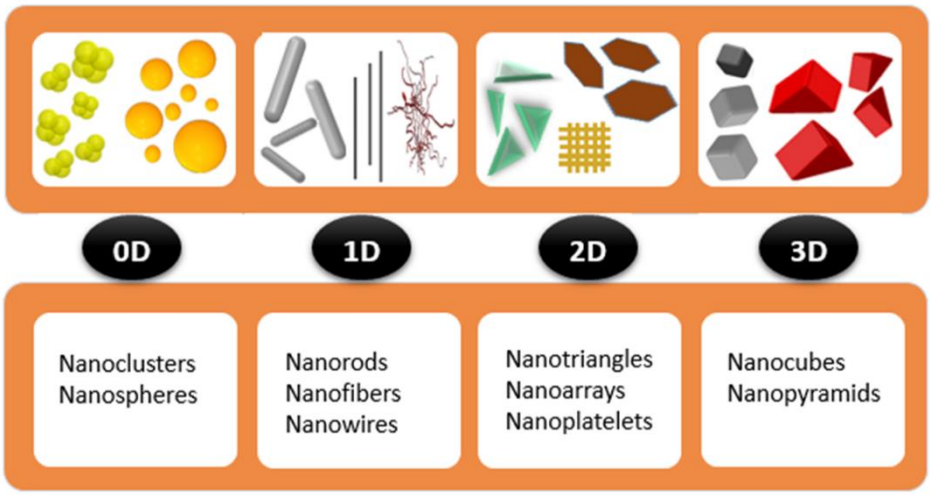

Figure 2.2 Nanoparticles of different dimensions

Applications of Nanoparticles based on dimension:

a) *1D Nanoparticles* are used in industries dealing with products that need or provide information storage systems, electronic products, sensors, fiber optics, biological drug delivery applications, etc.[42].
b) *2D Nanoparticles* can be used as emitters, in solar cells, heatsinks, superconductors, semiconductors, smoke filters, VCDs, water filters, composites, etc.

c) *3D Nanoparticles* can be applied in drug delivery applications as most of them are biologically active molecules, magnetic nanoparticle applications[43] also in nano-electronic devices.

2.1.2 Variation in Shape of the Nanoparticle

Most of the nanoparticles that have spherical shape (or as we can call them 'nanospheres') tend to have more of the amorphous nature. Crystal shaped nanoparticles (as in nano-crystalline whiskers) generally tend to have anisotropic nature.

By controlling the degree of variation in the shape, size and composition of the nanomaterials, customized nanomaterials can be achieved to fulfill the desired properties. Creating these next generation 'smart' materials with atomically engineered properties especially at nanoscale is an elusive challenge.

2.1.3 Variation in Aspect Ratio of the Nanoparticle

Shapes that have high aspect ratio are long and thin: Nanotubes, nanowires, nano belts, nanoribbons and nano coils.

Shapes that have low aspects ratio are those that are flat: Nano-platelets, nano-prisms, nano-cubes, nano-suspensions and colloids, etc.

2.1.4 Variation in Composition of the Nanoparticle

There are many ways in which one can vary the composition of the nanoparticles. Variations can be induced in the chemical nature of the nanoparticles, in their surface compositions, mixing states (internal as well as external), the oxidation state, etc.

There are a numerous methods for preparation of polymer nanoparticles, both at lab scale and industry scale. They are chosen based upon the required nanoparticle application, environment, manufacturing cost, quality, quantity and even the available manufacturing capabilities of the lab or firm. This is due to the fact the these nanopolymers can be produced by using the man-made processes such as dialysis, supercritical fluid technology, micro /mini / surfactant free emulsions, interfacial polymerization, etc.

2.1.5 Variation in Spherical Nature of the Nanoparticle

Polymer Nanoparticles generally have spherical shape with varying sphericity. This curvature of the surface of nanospheres plays an important role in determining their reactivity. These nanospheres may have different sizes and have different functionalities/moieties at their periphery. These functionalities can be changed and modified as per material property requirement. Nanopolymers in the shape of nanospheres, generally tend to react or adsorb other particles onto their surface. Another type of nanopolymers that do have spherical nature but are different from the nanospheres, are called as nanocapsules. These nanocapsule polymers act as cages to other molecules and have the capability to carry them around by encapsulating them.

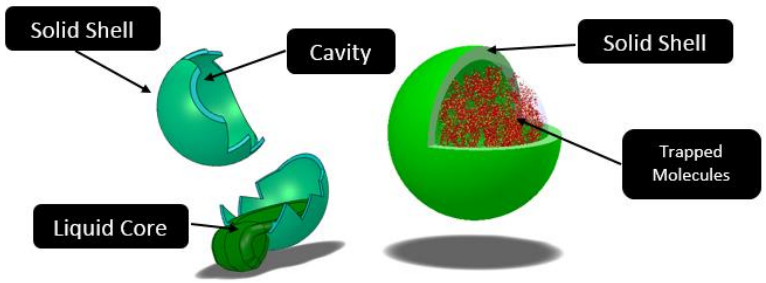

Figure 2.3 Encapsulation of molecules by polymer nanocapsules.

2.1.6 Challenges Associated With Modifying the Nanoparticle Architecture:

One important point that the researchers are still trying to understand is the loss of the expected properties when nanomaterials are embedded into macro or bulk matrices. For example in recent studies, researches answered these problems by changing the microstructure of the bulk matrix before nano materials are embedded into them. They embedded Nb nanowires that have a freestanding strain of up to 7 % into structurally altered NiTi SMAT matrix and this resulted in better properties of the matrix of almost up to 6% strain, as expected with nanowire insertion[44]. Though research on developing design guidelines for changing material architecture or topology of unit cells for unit cells of periodic cellular materials is available[45-47], extensive reconfirmation via experimentation is yet to be done.

In most of the materials used for engineering applications, strength is inversely proportional to toughness (or ductility). As the material's toughness increase the strength decreases and vice-versa. But from the above mentioned examples one can clearly conclude that this relationship between strength and toughness can be altered when one starts working with material architectures at nano scale.

2.1.7 Attempts in Tuning the Material Properties by Altering the Morphology.

By controlling the size and morphology of gold nanoparticles, researches have exploited the optical[48] , magnetic[49], electrical[50] properties of the nanoparticles. The shape of these nanoparticles are tuned and controlled to obtain anisotropy of the particle shape in order to exhibit the best optical properties and used them in applications like optical fibers, filters[4], biomedical devices[51], nano displays[9], sensors[52-53].

Block copolymers, dendrimers, 2D layers, nanofibers (NFs) and nanoparticles (NPs) are but a few of the chemically programmable materials that can be used to tune the properties of composite materials in nano, micro and even in macroscales. Morphology of materials can be altered by controlling their synthesis, by modifying their natural arrangement, by optimizing their ratios, and even by defining predestined positions to their assemblies.

Even at 2D level many attempts have been made to alter the morphology of the materials to bring out their potential properties. Researchers have tried to alter the morphologies of various available 2D materials such as graphene, silicene, germanene[54] etc., so as to understand how even simple changes in shapes can bring about unexpectedly deviations , especially betterment of properties. There have been attempts to form directed arrays where nanoparticles (NPs) on the surface of advanced 2D templates like graphene. This has been achieved through the introduction of programmable peptides as guiding agents, through which the position and quantity of the NPs was controlled. This 2D array of Nanoparticles which were arranged into their predestined locations on 2D graphene templates with the help of programmable peptides showed better electrocatalytic activity[55].

Nano-laminates (Cu–Ag laminates, Cu–Nb laminates) with high flow strength, high toughness, high plastic flow stability as well as high thermal stability have been successfully fabricated by controlling the layer thickness (CuZr layer)and modifying the interface interactions that include the structure of atoms, their arrangement and orientation and interface shear strength[56].

PEG polymers were grafted onto the surface of the silicon nanoparticles having azide or alkyl groups. These altered nanoparticles and nanoparticle arrays had enhanced water solubility and porosity and can be potentially be used in imaging, drug delivery and theranostic nano devices[57].

2.2 Design of Composites for Superior Stiffness & Strength

There have been theoretical attempts at studying the influence of nanofiller shape on the stiffness of the nanocomposite. In one particular study Styrene Ethylene Butylene Styrene (SEBS) was embedded with nanoscale tetrapod Quantum Dots (tQDs) and linear nanorods (NRs) and the change in Young's modulus of the nanocomposite was studied. Linear spring model (LSM) and experimental methods showed similar enhancement of nanocomposite toughness for both fillers. In fact, stiffness of the nanocomposite was more when tQDs were used as fillers in comparison with NRs. This increase in Young's modulus has been attributed to effective stress transfer through the matrix filler interface due to the isotropic branched shape of the tQDs (high probability of atleast one of the tQDs arms in tensile axis)[58].

Much research has been done to unravel the relation between the shapes of the nanofillers. In one particular literature, the polymer matrix was impregnated with fillers of different shapes and the variations in strength are studied. Molecular dynamics simulations were used to determine the breaking strength of the material. The three nanofiller shapes studied were icosahedra, rods, and sheets, out of which nanocomposites with 'sheet' like filler showed the best tensile strength[59]. As presented here, vast research on finding the relation between the nanofiller morphology and its influence on mechanical properties of

polymer matrix like stiffness and strength has been done and it was proven that it is very much possible to enhance these two properties together.

2.3 Design of Composites for Superior Toughness

To design composites with enhanced toughness is a complex and challenging task. Shear yielding mechanism of the matrix which in turn dissipates the energy determines its toughness[32]. Rigid fillers generally offer resistance to the moving crack front which again plays an important role in determining the fracture toughness of the composite along with stress concentration and debonding[60-61]. Embedding nanoparticles with low aspect ratio into the polymer matrix improves toughness of the nanocomposite. For example embedding amorphous polymers as fillers into the brittle thermoset matrices enhances their toughness[33].

Blending of thermosets with tough elastomers polymers has also shown remarkable improvement in toughness. For example, when diglycidyl ether of bisphenol A (DGEBA) epoxy resin was blended with amine-terminated polyoxypropylene (POPTA) elastomer, a remarkable improvement in the toughness of the epoxy was observed[62]. But in order to see significant improvement in mechanical properties via the technique of blending, a large amount of filler is required. This has a negative effect in terms of the nanocomposite cost, which is again undesired. Many attempts have been made to study the influence of filler morphology on the overall nanocomposite toughness. Layered fillers like organoclay have shown to increase the toughness of the composite[63]. This is due to exfoliation and intercalation of the epoxy matrices by addition of layered fillers[64]. Thus a delicate balance

between the type of filler, its loading percentage and cost needs to be monitored to achieve the required toughness in nanocomposites.

2.4 Nanocomposites with CNT and HBP Nanofillers:

Leveraging on the tubular structure of CNT and branched structure of hyperbranched nanomaterials many studies are conducted out of which a few are mentioned below.

Influence of CNT type, shape, specific surface area and chemical functionalization on the strength and stiffness has also been extensively studied and results showed improvement in both[65]. Influence of CNT dispersion on loss modulus, viscosity and storage modulus showed that better dispersion leads to better properties. Physical dispersion of nanofillers though has its perks of less labor and time, is not up to mark in achieving anticipated increase in mechanical properties at low loading levels. Poor interfacial bonding was seen in epoxies which were reinforced with CNTs without chemical treatment[66]. In order to minimize the interfacial gaps, researchers turned towards chemically modifying the CNTs before embedding them into polymer matrices. Chemical modification of CNTs with techniques like acid treatment, amine treatment and plasma oxidation proved efficient in increasing the epoxy nanocomposites tensile strength, elongation at break, viscosity, storage and loss moduli[67].

Effect of MWCNTs and SWCNTs on the mechanical properties of thermoplastic matrices also showed similar trends as in thermosets like increase in strength and stiffness but showed decrease in toughness[68-71]. When 2 weight percent (2 wt. %) MWCNTs were impregnated into relatively soft low density polyethylene(LDPE), mechanical strength

increased by 38 % but elongation at break and consequently toughness decreased by 75 %[72]. Amide terminated MWCNTs were functionally incorporated in polyurethane matrix and have shown improvement in tensile strength and thermal stability due to the improvement of polymer chain motion and excellent thermal stability of the CNTs[73]. This shows that no matter what the matrix is, though conventional CNT fillers increase strength and stiffness have a reverse effect on the toughness.

When epoxy functionalized HBPs were used as modifiers in epoxy at concentrations of 5, 10 and 20 parts per hundred, fracture surface increased but stiffness decreased by 10%. Optimal mechanical properties were obtained for medium functionalities of the HBP, to which finely dispersed particles correspond[74]. Hydroxyl functionalized hyperbranched polymer when blended with epoxy at 15 and 30 wt. % increased the fracture resistance with decline in elastic modulus. This was attributed to improved miscibility and compatibility between the HBP and matrix. Hyperbranched polyglycerol containing terminal five membered cyclic carbonate groups was synthesized and used to modify DGEBA epoxy. Addition of 20 wt. % and 40 wt. % HBP resulted in twofold enhancement of toughness in epoxy compared to neat HBP because micro particles were formed. However, flexural strength and stiffness were drastically reduced due to lack of phase separation[75].

There are multiple studies on functionalization of CNTs with hyperbranched polymers. Hydroxyl functionalized MWCNTs were used as growth supporter for grafting multi hydroxyl hyperbranched polyether's and showed good dispersion in polar solvents but no effort was made to determine the mechanical properties of the nanohybrids[76].

Similarly hyperbranched glycopolymers were grafted on the surface of MWCNTs by surface initiated atom transfer radical polymerization (ATRP) of 3-O-methacryloyl-1, 2:5, 6-di-O-isopropylidene-d-glucofuranose (MAIG) and water dispersibility was established[77].

Some studies use functionalized MWCNTs as reinforcements in hyperbranched polymer matrices. Macromolecules of hyperbranched polymers were grown on MWCNTs using the technique of self-condensing vinyl polymerization (SCVP) after the MWCNTs were functionalized with atom transfer radical polymerization (ATRP) initiators. Though good dispersion was shown by as prepared MWCNTs grafted with hyper branched polymers in THF and chloroform, no evidenced of mechanical property improvements were presented[78].

In other studies, multi hydroxyl functionalized MWCNTs were melt blended with acrylic acid grafted polyactide (PLA-g-AA) that improved thermal and mechanical properties but separation of organic or inorganic phase gave compatibility issues[79]. Nanocomposites of multiwalled carbon nanotubes and hyperbranched polyurethane (HBPU) were synthesized via click chemistry. It was found that the young's modulus increased by 191% and 140 % respectively at 2 and 4 wt. % loading. The good dispersion of MWCNTs into the polymer matrix and the substantial interfacial interactions between CNTs and the polymer matrix is the reason behind this significant impact on the mechanical properties[80]. Similarly, poly lactic acid-grafted multi walled carbon nanotubes (MWNT-g-PLA) were added to commercial PLA and improvements in tensile strength were observed. However, surface resistivity of MWCNTs prevented further enhancement

of tensile strength[81]. Hyperbranched polyborate (HBb) functionalized CNTs in polybenzoxazine showed improved thermal stability and good dispersion, but no in depth analysis about influence on mechanical properties was presented[82].

Thus as discussed above, combination of one or two properties is achievable i.e. superior stiffness, strength and toughness. However, it is challenging to realize a triumvirate of these properties. Specifically in composites, it is intricate to achieve high stiffness while not compromising on toughness. From the above literature search it can be seen that multifunctional 'Roding' nanofillers, synthesized from the combination of CNT's covalently coupled with HBP's which can improve the triumvirate properties as well as cure the epoxy are a novel and haven't been researched.

3 EXPERIMENTAL SECTION

3.1 Materials & Equipment

The thermoset option considered here as the matrix because it is commercially used in many mechanical, electrical and civil engineering applications. Araldite GY 6010 which is a Bisphenol A diglycidyl ether (DGEBA) epoxy and Modified Aliphatic amine Aradur 956-1 from Huntsman were used as the epoxy and hardener respectively.

Single walled Carbon Nanotubes from Sigma Aldrich (636797-1G), USA, of purity greater than 50 % are used. The diameter of tubes is 1.1 nm and length is between 0.5-100 nm.

Hyperbranched polymer of pseudo third generation with 32 terminal amine ($-NH_2$) functional groups was purchased from WeiHei Dendrimer Technology Co. Ltd, China. The

core of this hyperbranched polymer is ethane-1, 2 diamine core. Hyperbranched polymer of pseudo third generation with 32 terminal hydroxyl (-OH) functional groups, Boltron H30 was purchased from Polymer Factory, Sweden. The core of Boltron H30 is 2,2-bis(methyl) propionic acid and it is based on aliphatic polyesters[31].

Polytetrafluorethylene (PTFE) filter papers of pore size of 0.45 μm were purchased from Whatman USA. Mixed cellulose membranes of 47 mm diameter and pore size 0.45μm were purchased from Shangai Xinya purifier device factory. Vaccum filtration equipment and soxhlet extraction equipment was purchased from Sanaisi Ltd, China.

3.2 Characterization Techniques

Raman spectroscopy was carried out using Jobin Yvon Horiba Confocal Raman Spectrometer. 1064 nm laser beam was used for all filler samples in solid state.

TA Instruments Q50 Thermogravimetric Analyzer was used for TGA and with the Temperature range from 25 to 600 ^{0}C under nitrogen atmosphere. Heating rate was 5^{0}C per minute. Nitrogen purge rate was 20 ml/min and the weight of sample was 1g.

For XPS, the samples were loaded on Indium foils after removing any oxidized layer. XPS was performed using Kratos axis ultra XPS machine, in an ultra-high vaccum system using a monochromatic AL Kα source (1486.6 eV) at base pressure of $2x10^{(-10)}$ mbar.

The Rigaku Ultima III high resolution X-ray diffraction (XRD) was used to perform X-ray Diffraction technique. Scanning rate was kept constant at 2 min^{-1}, through a range of $2\theta=5^0$-60^0.

FTIR was performed using PerkinElmer FTIR 2000 spectrometer through a range of 400-4000cm^{-1}. Resolution was kept at 4 cm-1. CNT filler samples were dried, powdered and made into KBr pellets (at 0.1 wt% of CNT in KBr pellet). The pellets were made using a hydraulic hand press.

Tensile Test were carried out on Type V specimens using Instron in accordance with the standard ASTM D 638-10.

FE-SEM was performed using variable pressure scanning electron microscope S3400. The samples were sputter coated with platinum to a thickness of 3 nm.

3.3 Chemical Reaction Schemes

3.3.1 Carboxyl Functionalization of Carbon Nanotubes

In order to obtain superior physical properties of CNT/polymer composites, we need to purify CNTs to get rid of various impurities. Chemical modification not only contributes to the purification process, but also facilitates better dispersion of CNTs in polymer matrix. More specially, specific functional groups can be generated on the surface of CNTs through chemical modification. These tailored functional groups have an impact upon the structures and performances of CNT/polymer composites.

The following steps were followed to induce carboxyl functional groups onto the pristine CNTs. 100 mg of pristine SWCNTs were measured using an analytical balance and added to a to a 3:1 v/v 40 ml mixture of sulphuric acid (H_2SO_4 -98% concentration)and Nitric acid (HNO_3 of 65% concentration)and sonicated for 4 hours at 60 ^{0}C. The hot mixture of acids and CNT was left for 30 minutes at room temperature and was allowed to

cool down. Acid treated SWCNTs were then filtered using Polytetrafluoroethylene (PTFE) filter paper (pore size: 0.45 μm, 47 mm dia). The filtrate was then added in dropwise fashion to distilled cold water (deionized and PH-7) and washed continuously until the pH of the filtrate is neutral. PH level of CNT is critical as we want to ensure that washing removes all the traces of the acids. Obtained SWCNT-COOH were then placed in vaccum for 4h at heated at 80 ^{0}C so that all the water is evaporated. The oxidative corrosion of CNTs was followed in accordance with the literature[83].

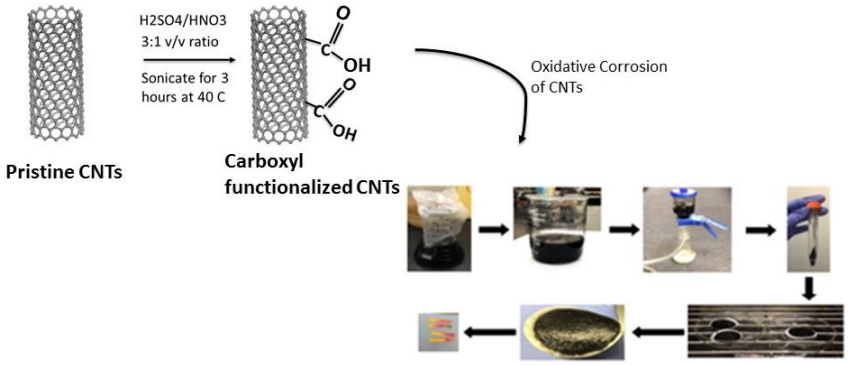

Figure 3.1 Carboxyl functionalization of CNTs

3.3.2 Amine Functionalization of Carbon Nanotubes

100 mg of CNT-COOH prepared in the previous step were dispersed in 100 ml of Ethylenediamine (EDA) for 2 hours till homogeneous dispersion was achieved. 10 mg 1-[Bis(dimethylamino)methylene]-1H-1,2,3-triazolo[4,5-b]pyridinium3-oxid hexafluorophosphate (HATU) was added to this mixture and the mixture was sonicated for another 6 hours. This mixture was subsequently diluted with 5 bed volumes of methanol and was filtered using polytetrafluoroethylene (PTFE) filter paper (pore size: 0.45 μm, 47 mm dia). The filtrate was then placed in the vaccum and dried at 80 ^{0}C for 4 hours. This

step completes the amine functionalization of SWCNTs and was carried out in accordance with the literature[84].

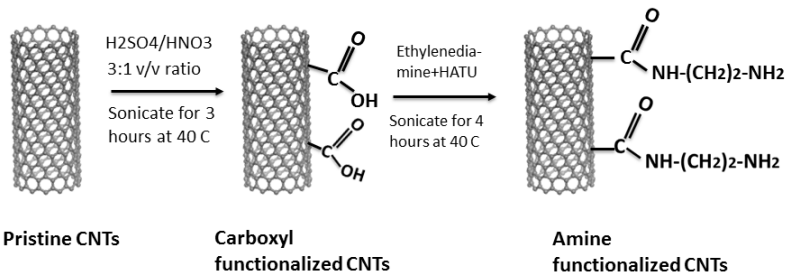

Figure 3.2 Amine functionalization of CNTs

3.3.3 EDC Coupling of Modified CNT and HBP

N-(3-Dimethylaminopropyl)-N′-ethylcarbodiimide hydrochloride also known as 'EDC' is one of the widely used coupling agents for coupling carboxyl and amine groups to form amide bond. 10 g of EDC was added to 100 ml of water. Acid treated SWCNTs (CNT-COOH) which were made from the previous mentioned procedure were dispersed in this mixture by the technique of ultrasonication. After uniform dispersion is achieved, 3.5 g of HBP which was prior dissolved in N,N-dimethylformamide (DMF) was added along into the mixture. The mixture was then stirred vigorously for 5~6 hours to get SWCNTs with amino groups on sidewalls as shown in the below figure. This step completes EDC coupling of CNT and HBP. However, filler samples using this procedure were not prepared because, as soon as HBP was added into water, the HBP and CNT separated out of the solution owing to their hydrophobic nature. This may have affected the efficiency of chemical bonding between them, which is undesirable.

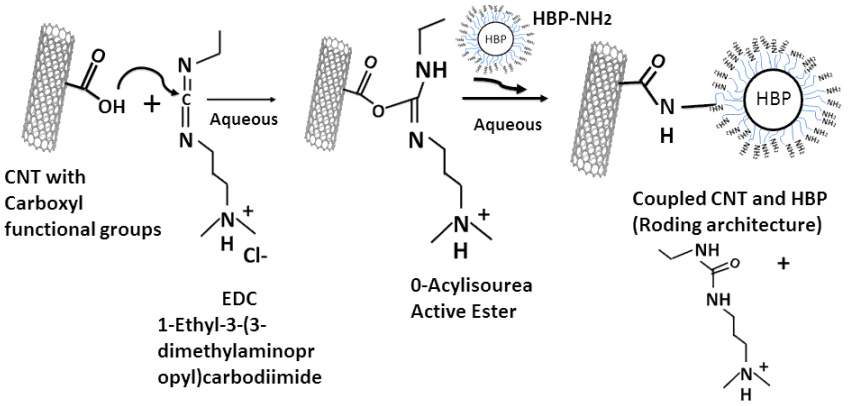

Figure 3.3 EDC coupling scheme

3.3.4 DCC Coupling of Modified CNT and HBP

Dicyclohexylcarbodiimide (DCC) is one of the very popular coupling agents that is used in the preparation of esters, anhydrides and amides from carboxylic acids. One of the main advantages of using DCC is that the byproduct formed as a result of the coupling reaction is generally insoluble in many common organic solvents and precipitates out of the mixture. This allows easy removal of the unwanted byproducts. This coupling agent is mainly used in solution phase reactions which is perfectly suitable for CNT nanofiller modifications.

100 mg of functionalized CNT-COOH was mixed with 50 ml of DMF and sonicated for 30 minutes. Simultaneously 3.5 g of HBP-NH_2 was added to 100 ml DMF and mixed for 1 hour using a magnetic stirrer. Uniform dispersion of CNT-COOH in the solvent was ensured before proceeding further. 10 g of Dicyclohexylcarbodiimide (DCC) was added to the mixture of CNT and DMF and sonicated for 30 minutes. HBP-NH_2 and DMF solution is then added to this mixture and was sonicated for 3 hours. The mixture was dispersed well for 6 hours by sonicating. After 6 hours, the solution was checked for precipitation of

CNT-HBP. If no precipitation occurred, the mixture was further mixed for 3 more hours. The mixture was then filtered with 10 bed volumes of DMF and then with water using a PFTE filter paper so as to remove the excess, unreacted HBP if any. The filtrate and water solution was placed into the centrifuge tubes and weight of each tube was measured carefully to make sure that they are equal. The mixture was centrifuged for 5-6 hours, to remove the excess solvent and in order to facilitate easy precipitation of HBP-CNT. The filtrate was then placed in a petri dish and dried for 8-9 hours.

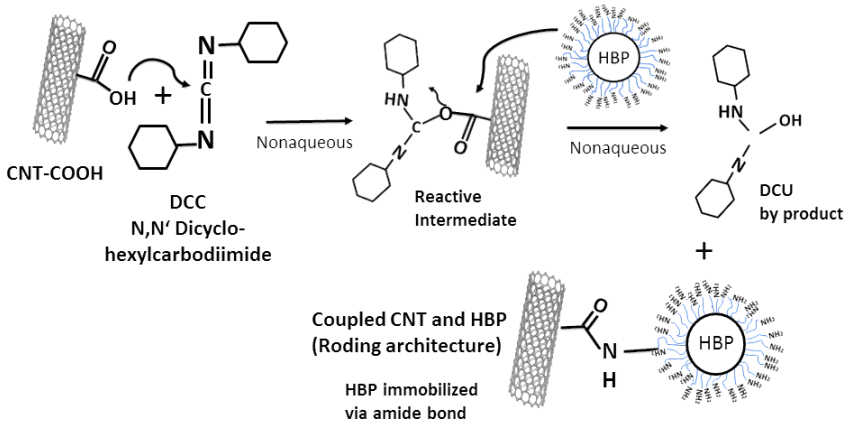

Figure 3.4 DCC coupling scheme

3.3.5 CDI Coupling of Modified CNT and HBP

100mg of support (which can be either be CNT-COOH or HBP-OH) was dispersed in 100 ml of DMF until uniform dispersion was achieved. In fume hood, 10g of Carbonyldiimidazole (CDI) was dissolved in 100ml of DMF while stirring with a magnetic stirrer. The support (functionalized CNT from the first step) was then added to the CDI solution and uniformly dispersed for 1 hour. Activated support (CNT-COOH / HBP-OH) was then washed with more than 10 bed volumes of DMF so as to thoroughly remove excess unreacted CDI and reaction by-products. CDI-activated support was then stored in

20 ml of DMF at 4 ^{0}C until required. CDI-activated support (CNT-COOH/HBP-OH) was filtered through a PFTE filter using a suction filter flask till the DMF is completely removed. Meanwhile nanoparticle containing amine functional group (HBP-NH_2 / CNT-NH_2) was dispersed in 100 ml DMF. Activated support (CNT-COOH / HBP-OH) which was filtered before was then added to this solution while stirring till uniform dispersion was achieved. The mixture was stirred for 24 hours using a magnetic bead. Depending on the amount of CNT and HBP being coupled, longer reaction times can be used if deemed appropriate. The mixture was then filtered using a suction filter flask and was washed extensively with more than 10 bed volumes of DMF and with water so as to remove excess unreacted HBP (if any) and the reaction byproducts. Once the vaccum was removed, the filtrate cake was broken into small pieces and suspended in water and further sonicated for 2 hours. Finally this mixture was filtered and the filtrate was dried in oven for 8 hours at 80 ^{0}C.

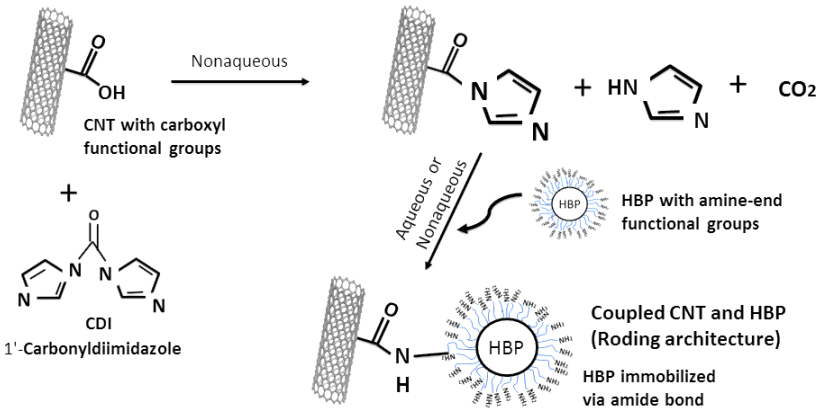

Figure 3.5 CDI coupling scheme for CNT-COOH and HBP-NH_2

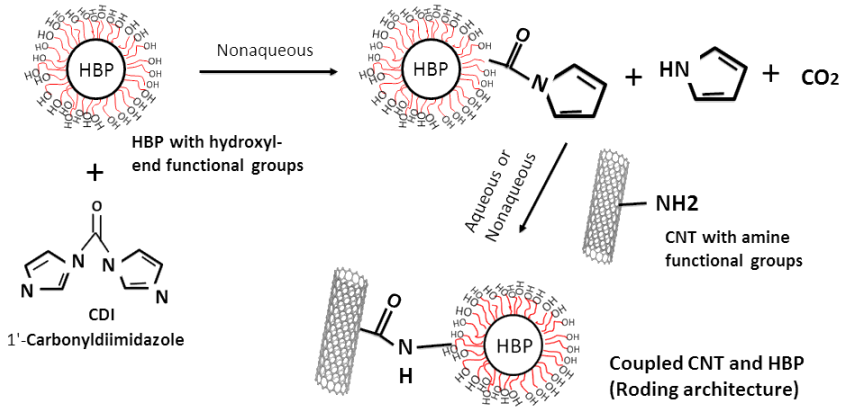

Figure 3.6 CDI coupling scheme for CNT-NH_2 and HBP-OH

Following the above coupling reactions, four nanofiller samples with different compositions of the 'Rod' like CNT and 'Damper' like HBP were prepared. The ratios of the constituent elements used to prepare the 'Roding' nanofiller sample are shown below.

Sample Name	Composition	Ratio	Coupling
S1	CNT-COOH & HBP-NH2	100mg:3.5g	CDI
S2	CNT-COOH & HBP-NH2	100mg:7g	CDI
S3	CNT-NH2 & HBP-OH	100mg:3.5g	CDI
S4	CNT-COOH & HBP-NH2	100mg:3.5g	DCC

Table 3-1 Roding nanofiller sample compositions

3.3.6 Preparation of DGEBA Epoxy Samples

15 g of DGEBA epoxy Araldite GY 6010 was uniformly mixed with 3.75 g of Aradur 956-1 amine hardener for 25 minutes using a magnetic stirrer. The mixture was then

degassed in vaccum for 10 minutes. Then it was cast into a silicon mold and placed in oven for 4 hours at 100 ^{0}C for curing.

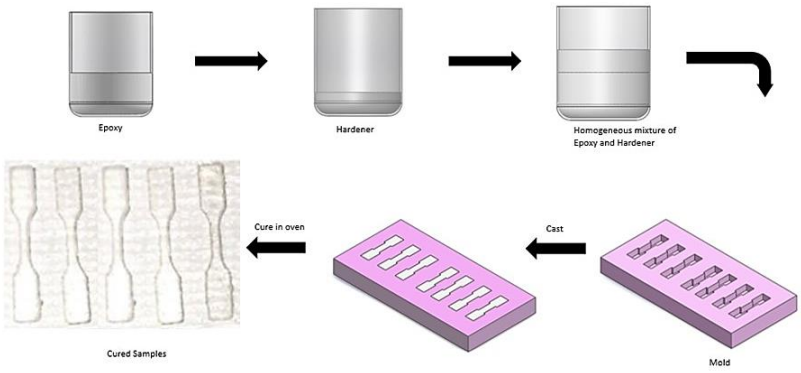

Figure 3.7 Pure DGEBA epoxy sample preparation procedure

3.3.7 Preparation of Epoxy Sample With Modified Nanofillers

According to different filler percentages and compositions, nanofillers were weighed precisely using an analytical balance. Then the filler was dispersed in 10 ml of acetone for 1 hour. This mixture was then added to 15 g of DGEBA epoxy and was mixed using a magnetic bead while heating at 70 ^{0}C for an hour, in order to evaporate acetone. Once all the acetone evaporates from the mixture, 3.75 g of Aradur 956-1 hardener was added and was further mixed for 25 minutes using a magnetic stirrer. The mixture was then degassed in vaccum. Then it was cast into a silicon mold and placed in oven for 4 hours at 100 ^{0}C for curing.

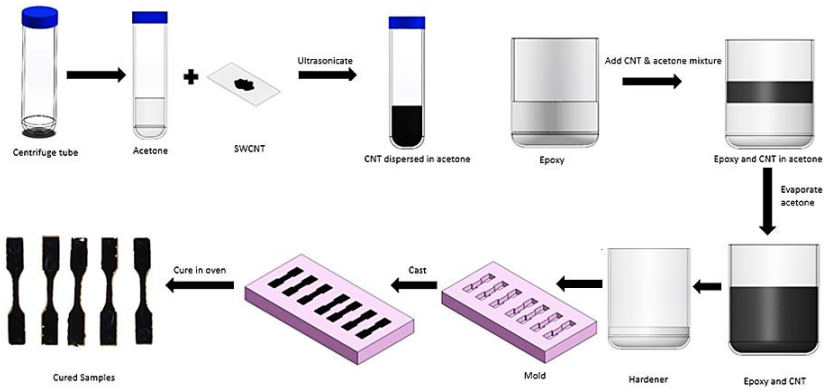

Figure 3.8 Nanocomposite preparation scheme

3.3.8 Preparation of Samples for Soxhlet Extraction

3g of DGEBA epoxy Araldite GY 6010 each was taken in four different aluminum pans and different amounts of HBP-NH_2 were added to it. Both were mixed for 10 minutes and the pans were placed in oven for 2 hours at 100 ^{0}C for curing. After two hours the samples were then placed in mixed cellulose membrane filter papers and wrapped into small packets.

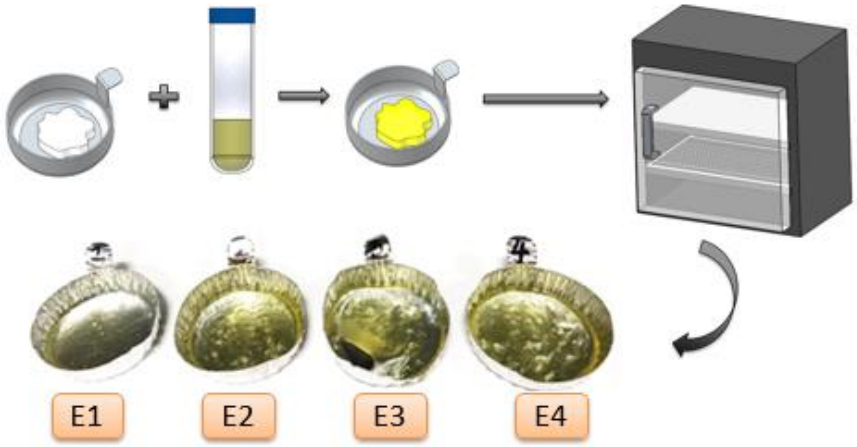

Figure 3.9 Soxhlet extraction procedure

Sample	Epoxy(g)	HBP (g)
E1	3	1.5
E2	3	3
E3	3	4.5
E4	3	6

Table 3-2 Sample compositions for soxhlet extraction

4 RESULTS AND DISCUSSION

4.1 Thermogravimetric Analysis

In this material characterization technique, the weight of the sample is monitored as a function of temperature and time. The sample is gradually heated through a temperature range in a controlled atmosphere till it starts degrading. TGA test is performed by placing the precisely weighed sample in the pan that is located inside the furnace. The sample is then purged with an inert or reactive gas and the changes in the weight of the sample are tracked along with time and temperature. This helps us to qualitatively figure out the loss

The existence of hyperbranched polymer on the modified single walled carbon nanotubes can be quantitatively found using thermogravimetric analysis. By comparing the TGA graphs of the pristine and modified CNT samples and HBP to the coupled samples, we can identify the existence of the amide bond between SWCNT and HBP. This can be done by calculating the weight loss percentages as well as the peak intensities of the graph.

4.1.1 TGA Results

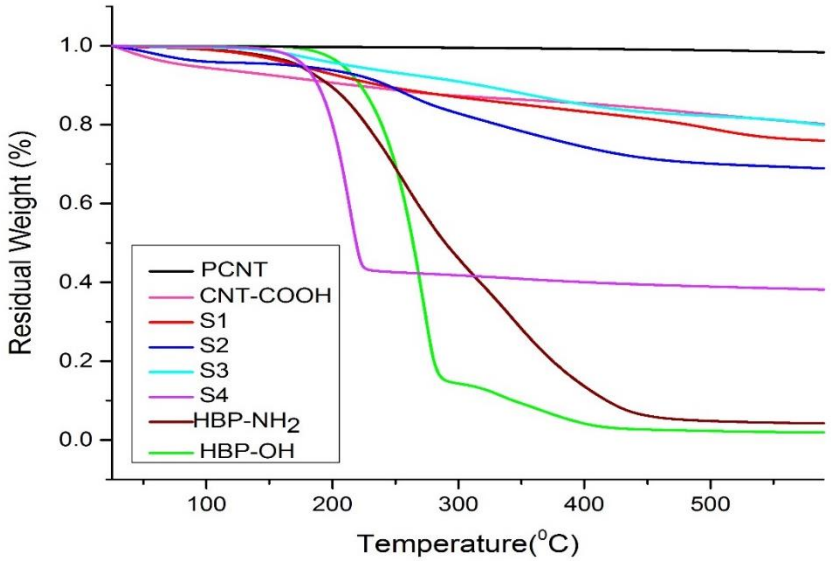

Figure 4.1 Residual weight vs. Temperature for (a) PCNT (b) CNT-COOH (c) S1 (d) S2 (e) S3 (f) S4 (g) HBP-NH2 (h) HBP-OH

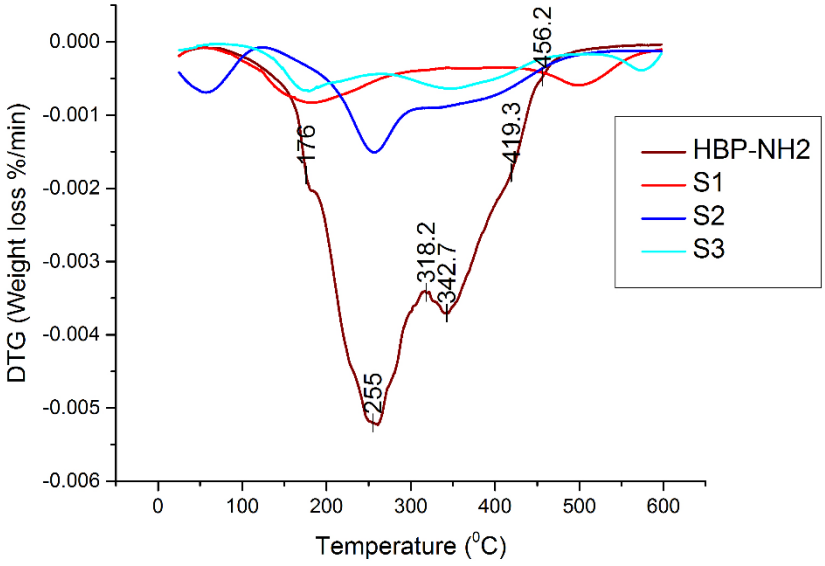

Figure 4.2 DTG peaks of (a) HBP-NH_2 (b) S1 (c) S2 (d) S3

4.1.2 TGA Analysis

a) From the above TGA graph it can be seen that for pristine CNT sample, the weight loss is almost negligible (weight loss of the sample was only 1.71 %). The sample

mass almost remains constant from the starting of the temperature range till 650 ^{0}C.This stability of the sample can be attributed to the very stable graphite structure of the CNTs[85]. Compared to pristine CNT, the carboxyl functionalized CNT showed more weight loss (20.05 %) and particularly significant weight loss was observed above 400 ^{0}C due to degradation of –COOH groups. These values are indicative of the fact that the thermal stability of the modified CNTs is much less than the pristine CNTs[86-87]. As the pristine CNTs are treated with strong acids to achieve CNT-COOH, oxidative corrosion of the tubes leads to the formation of defects on the CNT surface. These defects disrupt the graphitic structure of the CNTs and in turn lower their thermal stability.

b) *Peak Locations in DTG curve:* The DTG curve represents the derivative of the TGA curve with respect to time. In general DTG curves are used to find out the reasons for weight loss by co-relating the obtained peaks to the standard peaks of raw materials. We compare the peaks of the DTG curve for the coupled samples with curve obtained for HBP, to figure out if the degradation occurring in the coupled samples is actually because of the grafted HBP.

c) The mass loss occurring in the temperature range of 250-400 ^{0}C is mainly attributed to the thermal degradation of HBP (amidic groups)[85]. In this region, three peaks are observed in case of pure HBP. The same characteristic peaks can be identified in the coupled samples. This supports the interpretation that the weight loss in coupled samples is in fact due to the degradation of HBP present in the sample.

d) Another important observation is the increase in weight loss percentage between coupled samples S1 and S2. The coupled samples S1, S2 are prepared via CDI coupling reaction between carboxyl functionalized SWCNT and amine terminated HBP. Their weight loss percentages are 24.15 % and 31.19 % respectively. For both the samples the weight loss can be significantly observed in the temperature range of 200 ^{0}C to 400 ^{0}C. As amide bonds present in the sample are dislocated, the weight loss increases in the coupled samples when compared with the pristine CNT and CNT-COOH. This result clearly shows the successful grafting of HBP on the surface of CNT. The TGA graph and weight loss values obtained here are in well agreement with the literature[88] where CNT with amide interconnections showed a weight loss around 25 %, representing the degradation of amide groups. The researchers in the paper showed the proof that there is one added for every 50 Carbon atoms[88].

e) As mentioned above, the amount of HBP used for preparing sample S1 was half the amount used for sample S2. As more HBP is readily available to react with the functionalized CNT, it can be theoretically interpreted that the number of amide bonds formed in sample S2 (amide bong is the result of successful coupling between carboxyl group present on CNT-COOH and amine group present on HBP-NH_2) will be more in comparison with sample S1. It can be predicted that as S2 has more HBP covalently attached to the CNT, then the weight loss of the sample should be more. By comparing the obtained weight loss percentages of S1 (24.15 %) and S2 (31.19%) this prediction can be proved. Percentage weight loss of

sample S3 on the other hand, is very less, that means there is more CNT-NH_2 and less HBP-OH in the sample. This result shows that though the covalent bonding is successful, it is not to the expected levels. Lower coupling in S3 can be attributed to the difficulty in reactivity of the –NH_2 group present on the CNT (in comparison with the –NH_2 group in HBP). This results are on par with the elemental composition values of samples as can be seen from XPS data, in later sections.

Sample	Weight before TGA (g)	Weight after TGA (g)	% Weight Reduction
Pristine CNT	1	0.9829	1.71
CNT-COOH	1	0.79949	20.051
S1	1	0.75855	24.145
S2	1	0.68812	31.188
S3	1	0.79763	20.237
S4	1	0.38091	61.909
HBP-OH	1	0.01884	98.116
HBP-NH_2	1	0.04195	95.805

Table 4-1 Percentage weight reduction calculations

f) *Elimination of S4:* From the above table, we can observe that the percentage weight loss for S4 is very high. That means, there is a high amount of HBP-NH_2 present in the sample. This can be reconfirmed by comparing with XPS data for S4, we can

see that nitrogen element which represents HBP in the sample is very high. This high weight loss of the sample is undesired. So sample S4 has been eliminated from other characterizations.

g) The major take away from the TGA analysis are summarized as: Additional mass loss observed in the coupled samples is due to the existence of HBP linked to CNT via amide bond. The more the presence of HBP in the filler, the less will be its thermal stability.

4.2 X-Ray Diffraction

In this technique, the filament present in the cathode ray tube is heated up, which results in emissions of electrons. These electrons are then focused onto the sample. As soon as the accelerated electrons strike the sample, the existing electrons in the surface and inner shells of the sample are replaced or disturbed, producing X-ray spectra. These X-ray spectra are characteristic to the sample's crystallinity and composition.

In this research, XRD technique was used to determine the nature of the modified 'Roding' nanofillers. The pristine CNT are generally crystalline in nature and hyperbranched polymers are amorphous in nature. So in comparison with pristine CNT, the crystallinity of the 'Roding' nanofillers should decrease (owing to the increase in amorphous nature due to grafting of HBP onto the CNT surface). Apart from determining the nature of the sample, XRD can also be used to determine the sample purity.

4.2.1 XRD Results

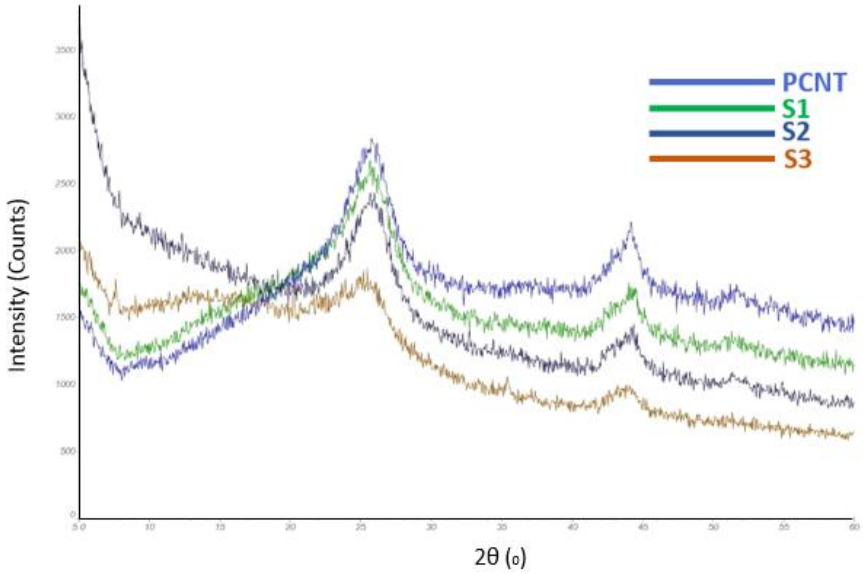

Figure 4.3 XRD peaks of (a) Pristine CNT (b) S1 (c) S2 (d) S3

4.2.2 XRD Analysis

a) *Location of Peaks:* The XRD peaks around 26.5^0 represent the (002) hexagonal plane of graphitic lattice. The peak at 42^0 represents (100) peak of hexagonal graphite[89].It can be clearly seen that the peak for (002) plane shifts towards left in the coupled samples S1, S2 and S3. Another observation is that the peaks become broader as the amount of HBP grafted onto the SWCNT surface increases. This result is in par with literature where the broader peaks were attributed to increasing disorder in the CNT lattice of the sample[89].

b) *Peak Intensities:* Apart from the shift of the 2θ peaks, difference in intensities at 26.5^0 and 42^0 can also be observed. The XRD peak intensity of the coupled samples S1, S2, S3 decreases in comparison to pristine CNT due to an increase in disorder which points to functionalization with amorphous HBP (representing the

amorphous nature increases). At the places of disorder in the CNT lattice soft HBP is bonded via covalent linkage to the surface of SWCNTs[89]. This XRD result shows that coupling has indeed been successful and the 'Roding' architecture is formed in the CNT-HBP coupled samples. Thus we can prove using XRD technique that, there is interaction between the hyperbranched polymer and CNT[90].

c) *Elimination of S3*: The peaks for sample S3 are very broad representing high disorder in the CNT lattice. This is undesirable as disrupting the CNT lattice too much can potentially decrease the strength and stiffness of the filler. So, sample S3 has been eliminated from all the further characterizations.

4.3 Fourier Transform Infrared Spectroscopy

In Fourier Transform Infrared Spectroscopy, the monochromatic IR radiation is focused through a sample. As the light passes through the sample, some of it is either absorbed or deflected or emitted (due to emission of photons from the sample). Thus, the emitted light is captured and analyzed. Each bond present in the sample generally has a characteristic vibrational frequency. This frequency is reflected as peaks in the IR spectra. The analysis of these peaks can provide us with both qualitative and quantitative idea about the sample. The transmission and absorption spectra are one of the best fingerprints for functional group and chemical bond analysis due to their accuracy as well as simplicity. Different functional groups present in the sample can be analyzed using FTIR. When pristine carbon nanotubes are modified, different functional groups according to the chemistry of modification result on the tubes. By observing the peaks produced by the IR spectra, we can analyzed the success of the chemical reaction.

In this research, the pristine and modified CNTs are powdered and diluted with KBr to make KBR pellets before they are placed in the machine.

4.3.1 FTIR Results

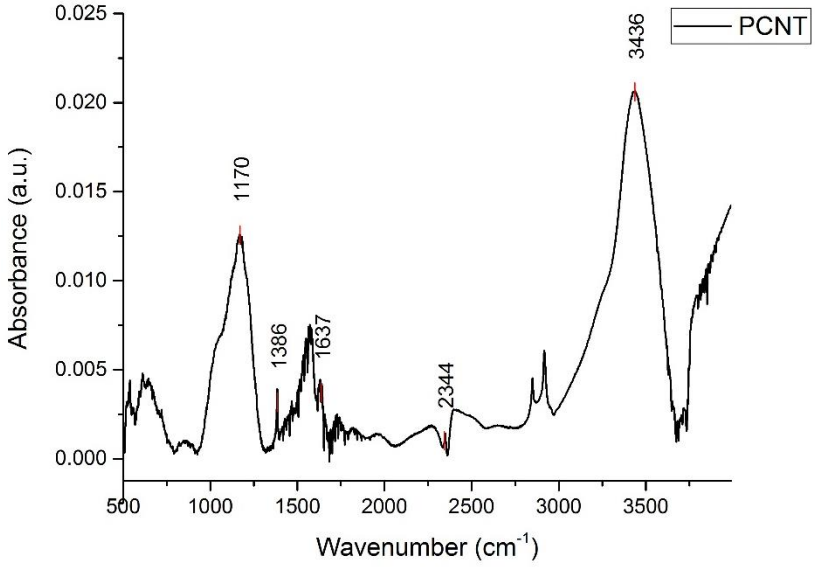

Figure 4.4 FTIR of Pristine CNT

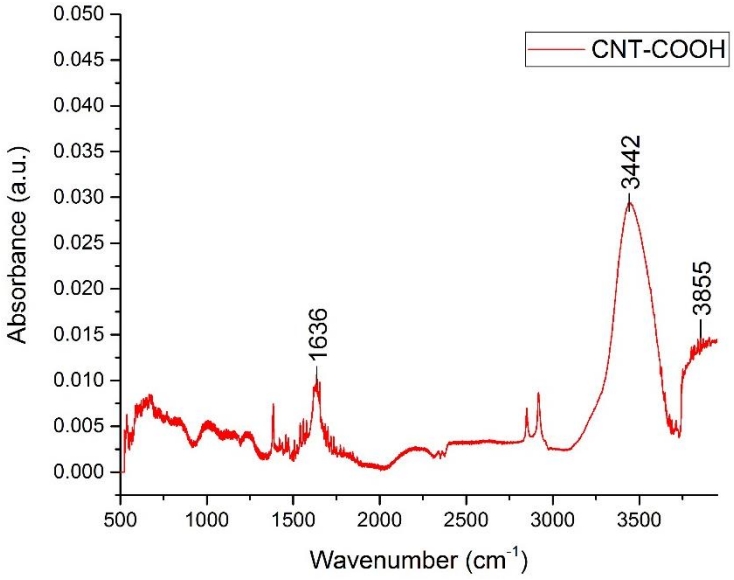

Figure 4.5 FTIR of CNT-COOH

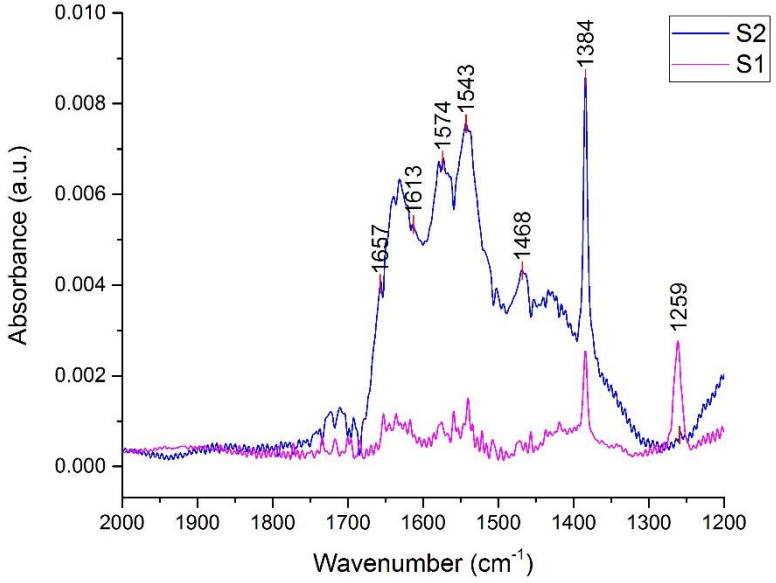

Figure 4.6 FTIR of samples (a) S1 (b) S2

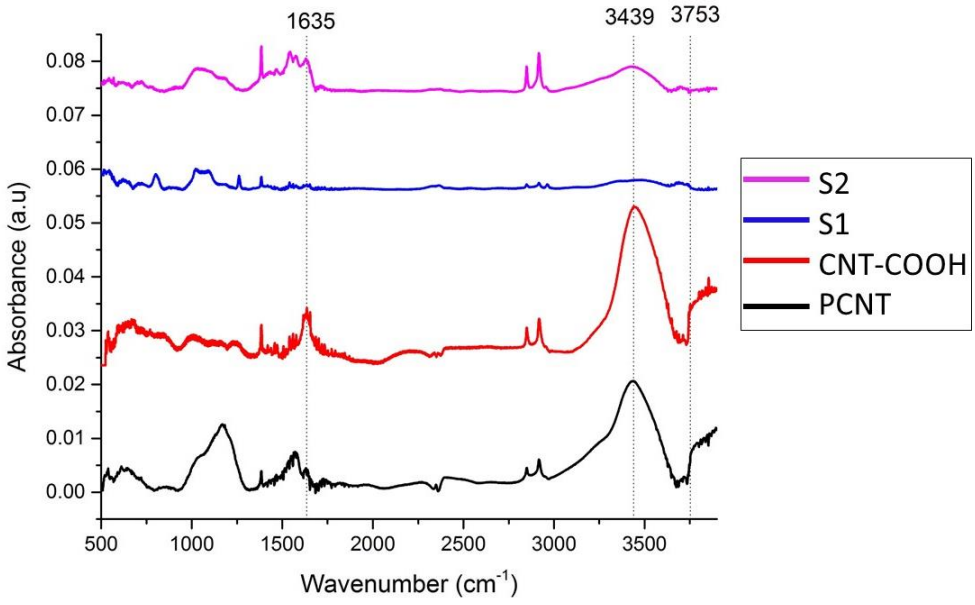

Figure 4.7 FTIR Spectra for (a) Pristine CNT (b) CNT-COOH (c) S1 (d) S2

4.3.2 FTIR Analysis

a) *FTIR Spectra for Pristine CNT:* Peak at 1170 cm^{-1} represents C-O stretching[91], peaks at 1386 cm^{-1} and at 1637 cm^{-1} represent C=C stretching[92], peak at 2344 cm^{-1} can be attributed to CNT backbone stretching[93] and peak at 3436 cm^{-1} can be attributed to adsorbed atmospheric moisture.

b) *FTIR Spectra for CNT-COOH*: This spectra shows the peaks at 1640 cm^{-1} which can be attributed to carbonyl (C=O) group[94], 3439 cm^{-1} which can be attributed to free hydroxyl (–OH) stretching and at 3753 cm^{-1} which can be attributed to carboxyl (–COOH) group[95].

c) *FTIR Spectra for S1 & S2:* Samples S1 and S2 are prepared by coupling HBP-NH2 and CNT-COOH via amide bond. Just like expected, for both the coupled samples S1 and S2, the sharp peaks typically ascribed to amide bond can be seen. The peak at 1657 cm^{-1} can be attributed to amide C=O stretching, peak at 1613 cm^{-1} represents amide N-H stretching, peak at 1543 cm^{-1} shows amide C-N stretching vibration, peak 1468 cm^{-1} shows amide N-H bending, peak at 1348 cm^{-1} can be attributed to amide C-N stretching and peak at 1259 cm^{-1} shows out of plane amide N-H deformation[88]. All these peaks indicate that the strong interaction between HBP-NH_2 and CNT-COOH is indeed due to irreversible covalent amide bond.

d) *Comparison of the FTIR Spectra:* To examine the formation of covalent amide bond between CNT-COOH and HBP-NH_2, control samples from pristine PCNT and CNT-COOH have been prepared. As it can be seen from the stacked spectra graph, peaks at 3439 cm^{-1}, 3753 cm^{-1} represent free or unreacted –OH and –COOH

groups respectively. By comparison of the intensities, it can be seen that these peaks gradually disappear in S1 & S2 showing that all the –OH and –COOH have reacted with $–NH_2$ group from HBP to form amide bond. Peak at 1635 cm^{-1} represents C=C stretching from CNT backbone and remains intact even in spectra of S1 & S2.

4.4 X-ray Photoelectron Spectroscopy

X-Ray photo electron spectroscopy or as it is widely known, XPS is a non-destructive characterization technique that is based on the principles of Einstein's 'Photoelectron Effect'. It helps us in identifying the chemical com position of the sample, Quantitative surface composition, Chemical state of the sample constituents the chemistry and lateral distribution of the surface elements. When the incident X-Ray beam that comprises of photon hits the sample surface, it is absorbed by the sensitive sample's surface and photoelectrons are ejected from that sample. The notable point here is that each electron that is ejected from the sample's surface has a specific kinetic energy. We try to quantify these photo-ejected electrons along with their kinetic energies to better understand the sample's composition. The nature of bonds can be identified by calculating the binding energy of the ejected electrons using the conservation of energy principle. We can find the binding energy of the electron using the following formula:

$$E_{binding} = E_{photon} + (E_{kinetic} + \phi)$$

Where,

E binding = The Binding energy of the electron before it was ejected.

E photon = Energy of the incident X-Ray beam.

E kinetic = Kinetic energy of the ejected electron.

Φ = Work function of the electron that was ejected.

Subtracting the kinetic energy of the photo ejected electron and the work function of the electron (which is the energy required to remove the electron from the sample surface into the vaccum that surrounds the sample) from the already known value of the incident X-ray beam energy (E photon) that is being incident on the sample surface, provides us with a quantifiable value of the Kinetic energy of the ejected electron.

In order to examine the success of the coupling reaction, X-Ray photoelectron Spectroscopy (XPS) was used. XPS helps in analyzing the chemical composition of the sample by providing a fingerprint of the elements present in the sample. Furthermore XPS can also be used to characterize the electronic structure of the sample. It is relevant to do XPS for ‘Roding ‘nanoparticles as the elemental mapping provided by XPS can be used to identify the chemical composition of the SWCNT surface. The escape depth of the electron when using XPS is approximately 10 nm and that is more than enough to provide elemental information of the modified CNT surface. Along with the finger print of the surface of modified CNT, we can quantitatively figure out the exact composition and the percentage of chemical modification that has taken place. In other words we can find out if the HBP is present on the CNT surface and if it is the amount of HBP present. This information of the type of chemical bonding can help us to better understand the success of the coupling reaction. Each ejected electron has a specific energy associated with it sand studying these energy that are represented by peaks in the graph, which give us a better understanding of

the chemical composition. The surface elements present on the modified CNT can be identified by the intensity and energy of the peaks. The characteristic binding energies help us in recognizing the elements present on the SWCNT surface. In order to obtain the concentration of the elements present on the SWCNT surface we analyze the area of the peaks.

Using this technique we can find out the existence of chemicals like Carbon, Nitrogen and Oxygen. The X-axis of XPS survey spectra graph represents the binding energy of the ejected electrons. As can be observed in the graphs below the X-axis is in decreasing order i.e. the binding energy value is more when closer to the Y-axis and decreases gradually. The reason behind this is that reversed energy representation provides a better representation of the atom structure.

4.4.1 XPS Results

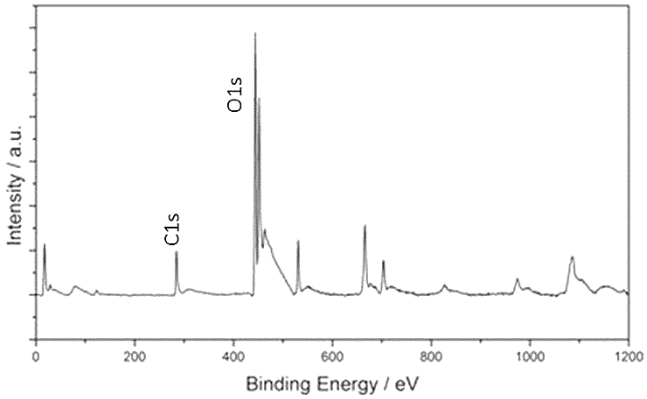

Figure 4.8 XPS survey spectra of pristine CNT

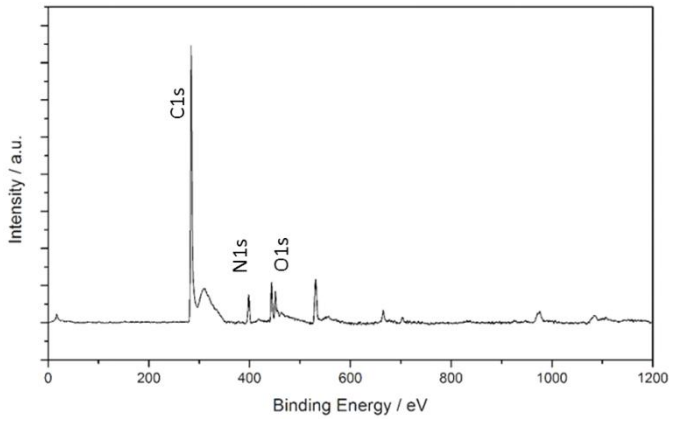

Figure 4.9 XPS survey spectra of sample S1

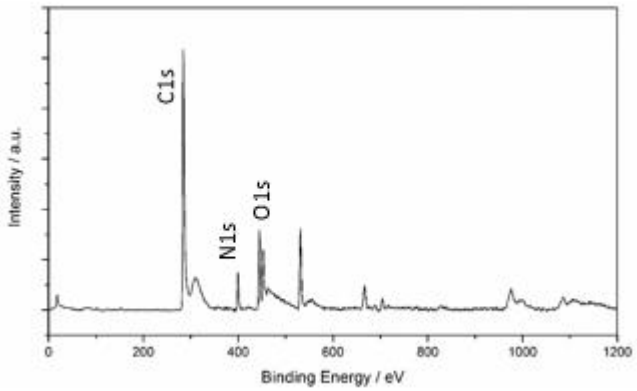

Figure 4.10 XPS survey spectra of sample S2

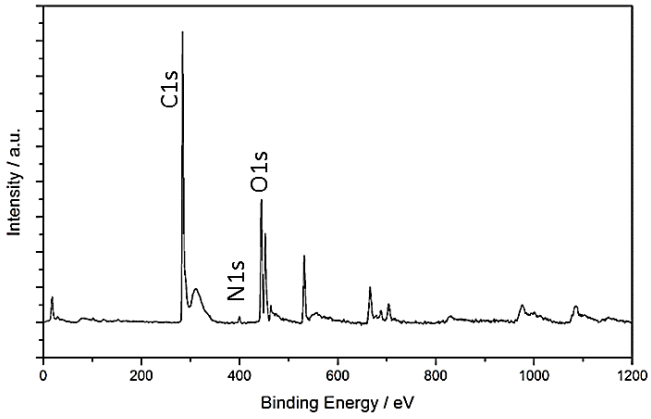

Figure 4.11 XPS survey spectra for sample S3

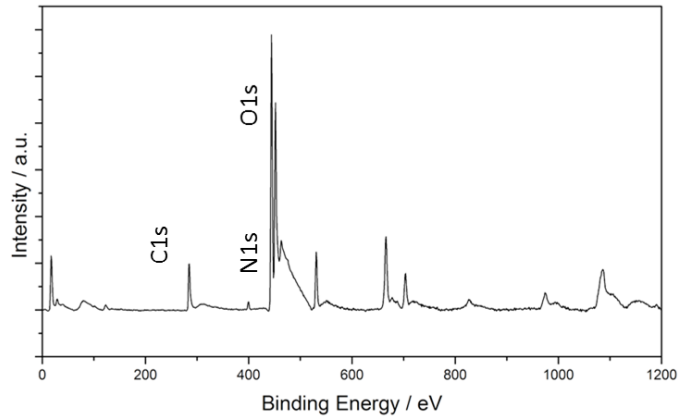

Figure 4.12 XPS survey spectra for sample S4

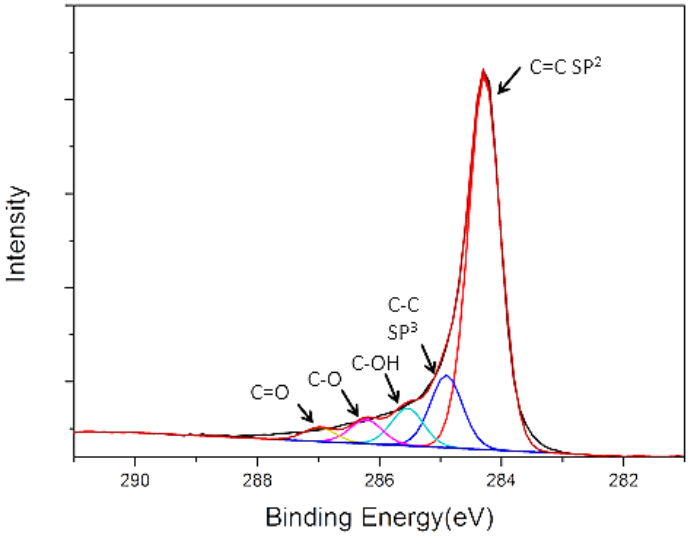

Figure 4.13 Peak separations of pristine CNT.

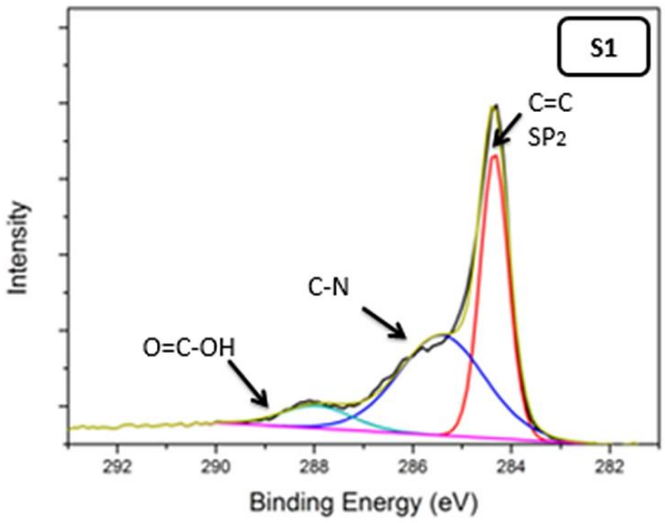

Figure 4.14 Peak separations of sample S1

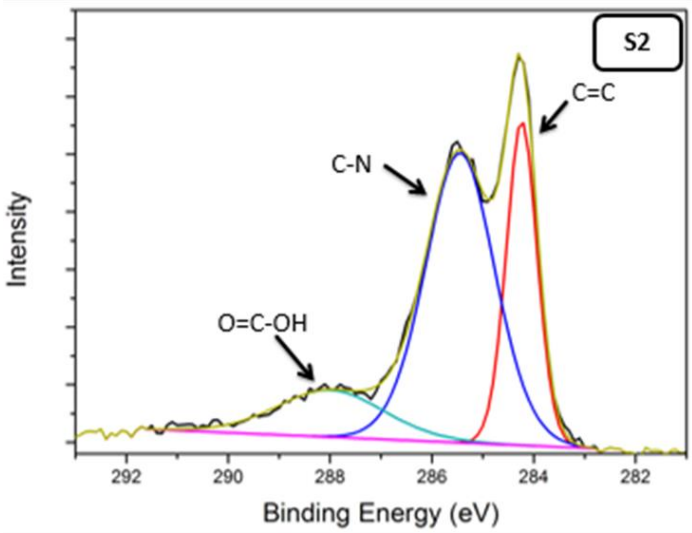

Figure 4.15 Peak separations of sample S2

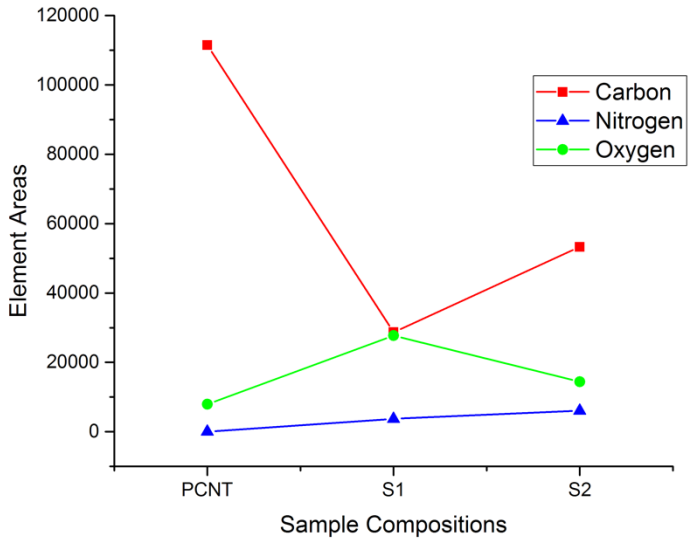

Figure 4.16 XPS elemental areas for (a) Pristine CNT (b) S1 (c) S2

4.4.2 XPS Analysis

a) *XPS survey spectra of pristine CNT:* In pristine CNT only carbon and oxygen are present as seen from the graphs. This oxygen in the pristine sample comes from the impurities and unavoidable moisture adsorption that occurs during the manufacturing. This obtained oxygen valued is on par with the purity of the CNT samples.

b) *XPS survey spectra of S1, S2, S3 & S4:* The location of the carbon element peak in XPS survey spectra of all the samples is between 250~300 cm^{-1}. Oxygen peak is located around ~550 cm^{-1}. The samples S1, S2, S3, S4 all have nitrogen element present in them, thus they have the peak at the location of ~400cm^{-1}. This proves successful grafting of HBP onto the CNT surface.

c) *Deconvolution of XPS Peaks:* The significance of the deconvoluted are shown in the graph. This is in correspondence with literature[96].C-N peak intensity for sample S2 is greater than sample S1. This is expected as more HBP-NH_2 was used to make S2 in comparison with S1, resulting in increased possibility for grafting. This is in par with XRD and Raman spectroscopy results.

d) The deconvolution of the spectra of S1 and S2 clearly show the existence of amide bong between CNT and HBP, reconfirming the success of formation of 'Roding' architecture in the hybrid filler.

e) *Area under the peaks:* The area of the peak and the intensity of the peak provides a quantifiable idea about the relative portion of the elements attached to the CNT surface. As stated earlier, the HBP used to make the sample S2 is double than the HBP used to make sample S1. So it is natural to expect double the amount of HBP grafted onto the SWCNT surface. As per expectations, we can see that the ratio of HBP grafted onto the surface of CNT in sample S2 is almost double the amount of HBP grafted onto sample S1.

Element	Pristine CNT	Sample S1	Sample S2	Sample S3	Sample S4
O	7933.68	27718.33	14429.41	17647.96	12990.66
C	111460.45	28689.58	53306.97	82199.83	72471.193

N	0	370 7.07	609 2.092	177 5.549	718 7.439

Table 4-2 XPS peak areas

d) From observing the area under the peak value of sample S3 we can see that the value of Nitrogen (representing amide bond/covalent coupling between CNT and HBP) present in the sample is very low. That means that the coupling technique is successful but not to the extent where we can expect the dampening effect from HBP. This result shows that there is a very low percentage of HBP grafting onto the CNT surface. This is mainly because of two reasons. It is very difficult for HBP-OH to react with the amine group present in CNT-NH_2. This is due to the fact that the length amine group bond length of the CNT surface is very small and it is not readily available to react with other groups. (In comparison with the bond length of the amine moieties at terminal ends on HBP-NH_2 arms in other samples). The reach of the functional groups is influences by the excluded volume of the hyperbranched polymers[31].

4.5 Raman Spectroscopy

It is one of the most popular spectroscopy techniques used for characterization, in which monochromatic light scattering is analyzed to get information about the sample. Light from laser is used for focusing on the sample because of its high intensity. This intensity of the laser can potentially amplify the results and make it easier for the observer to analyze the results. When the monochromatic light from a laser strikes the sample, it is scattered. And this scattering occurs because there is a particular frequency associated with

the photons present in the incident the incident monochromatic light, and it changes once the light interacts with the sample. The sample absorbs a few of the photons from the incident monochromatic light and re-emits them. The light emitted from the sample is what has all the information that we are looking for due to its shifted nature. The re-emitted light is collected and its frequency analyzed. Due to the interaction with the sample, the frequency of around 10-5 % of the reemitted light is either more or less in comparison with the incident light's frequency. The vibrational state of the sample is what determines whether the re-emitted light will have more or less frequency. Every molecule in the sample has an electron cloud around it in the form of an ellipsoid. When the monochromatic light touches the sample, this cloud's vibration energy is altered and that alteration results in the production of bands in Raman graph. The modified carbon nanotubes along with the pristine nanotubes were characterized using the Raman spectroscopy technique.

4.5.1 Raman Results

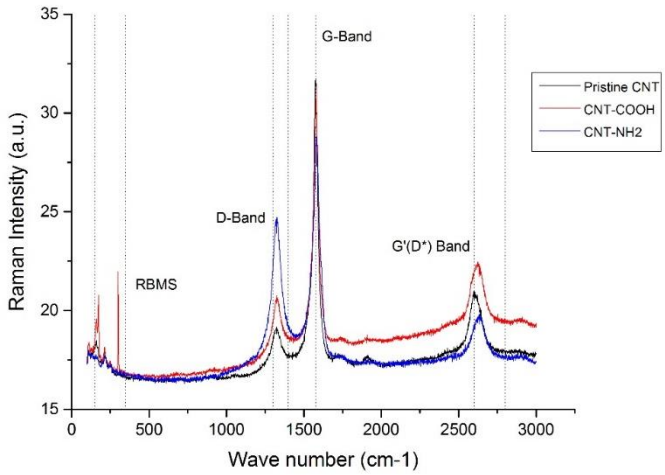

Figure 4.17 Raman spectra of (a) Pristine CNT (b) CNT-COOH (c) CNT-NH_2

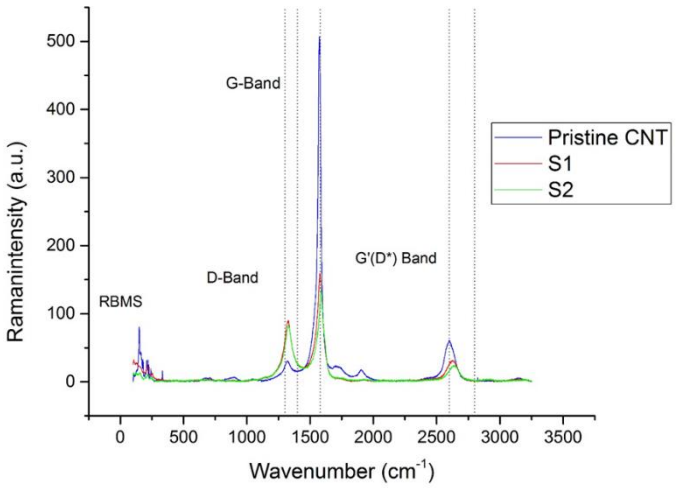

Figure 4.18 Raman spectroscopy of (a) Pristine CNT (b) S1 (c) S2

4.5.2 Raman Analysis

As it can be observed in the graph, there are four main bands obtained when SWCNTs are characterized using Raman spectroscopy. Each of these bands convey different results. They have be listed pointwise for clear understanding.

a) *Intensities of bands:* The D band (defect band) intensities have increased for both the carboxyl and amine functionalized CNTs. As D-band represents the defects in the structure of the carbon nanotube, it can thus be interpreted that the functionalization process was indeed successful. Intensity of D Band is more for sample S2 than sample S1. This means that the nanotubes of sample S2 have more defects in their structure (representing there is more HBP attached to the S2 surface) than S1[86]. This is expected because more hyperbranched polymer was used in the preparation of S2.

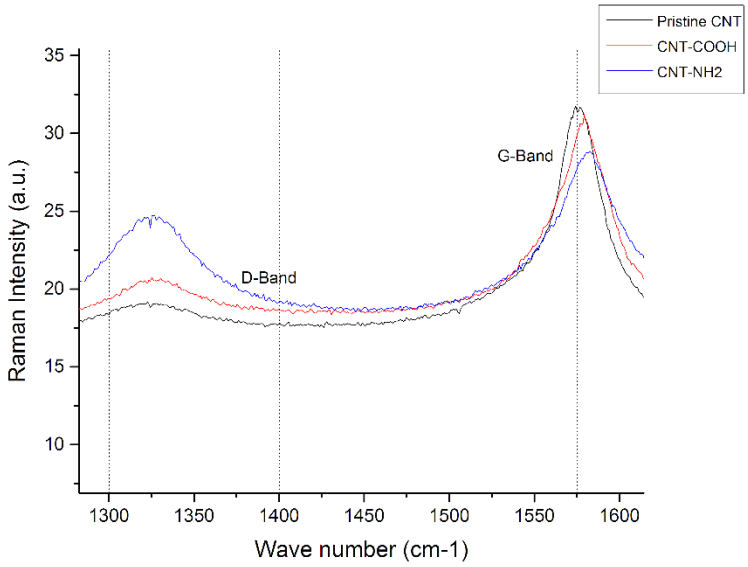

Figure 4.19 D-band & G-band intensities of (a) Pristine CNT (b) CNT-COOH (c) CNT-NH_2

G-band intensity represents the loss of electrical resonance. Intensity of G-band increases in the amine and hydroxyl functionalized CNTs when compared to pristine CNTs. This is due to the fact during the process of oxidative functionalization and filtration of CNTs, the amorphous CNTs is removed. This results in increase in crystallinity of the sample that id reflected by increase in G band intensity. The intensity of band is less for S2 when compared with S1. It shows that that as the S2 sample has more amorphous HBP attached to its surface, it is less crystalline than S1[87].

b) *Variation in shape of the graph/Raman shift:* The slight variations observed in the shape of the spectra of modified CNTs represent that their structure is different from the pristine samples[87] .Also there is a slight shift in the bands of modified samples when compared to the pristine CNT sample. This shows that there is a

change in the morphology of coupled CNT samples S1 & S2. The amounts of shifts in the D Band and G Band peaks are listed in the table below:

Samples	X_D cm^{-1}	Y_D cm^{-1}	X_G cm^{-1}	Y_G cm^{-1}
Pristine CNT	1329.78	29.500	1572.870	506.849
S1	1328.92	89.925	1577.934	159.442
S2	1330.62	83.280	1588.060	134.911

Table 4-3 Raman band peak locations

c) *I_D/I_G Ratio or R value*: This is the ratio of integral areas of D and G band peaks and it represents the structural disorder of the nanotube sample. R value increases with increase in structural disorder[88].This can be clearly observed between S1 and S2. Sample S2 has more HBP grafted onto its surface and thus has more structural disorder than S1.

Samples	I_D	I_G	$R=I_D/I_G$	1/R
P-CNT	1139.75	19259	0.0591	16.897
S1	5558.33	9395.05	0.5917	1.69026
S2	5024.81	7388.87	0.680	1.4704

Table 4-4 Integral band areas and R values

d) *Radial Breathing Modes (RBMs):* RBMs are observed especially in single walled nanotubes in between 150 to 350 cm^{-1}. A clear difference in RBMs of modified CNTs and pristine CNT is observes, which signifies that there is a new material has been grafted onto CNT structure during the functionalization process[97].

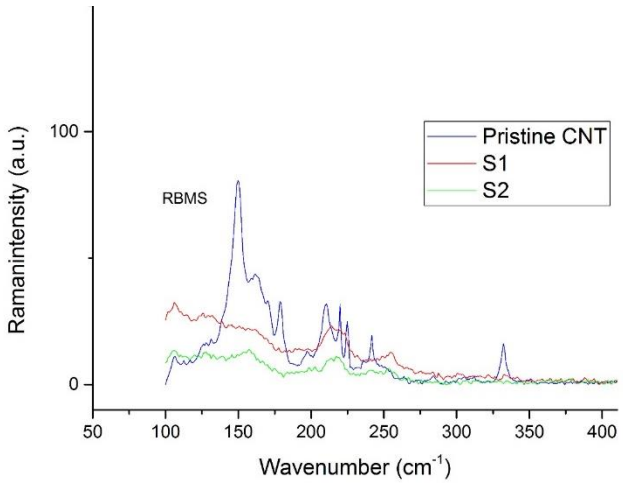

Figure 4.20 RBMS for (a) Pristine CNT (b) S1 (c) S2

e) *Elimination of S1:* By comparing the XPS and Raman results for samples S1 & S2, it can be observed the amount of HBP-CNT coupling is significantly higher in sample S2. Thus, the sample S2 was used as 'Roding' filler to make the nanocomposite samples to test the mechanical properties.

4.6 Tensile Test

Tensile test is performed to analyze the mechanical strength, stiffness, toughness and elongation at break of nanocomposites embedded with 'Roding' nanofillers. Control samples of pure epoxy (no nanofiller) were prepared. The test was done according to ASTM D 638-10.

4.6.1 Tensile Test Results

a) For filler loading of 0.25 weight%

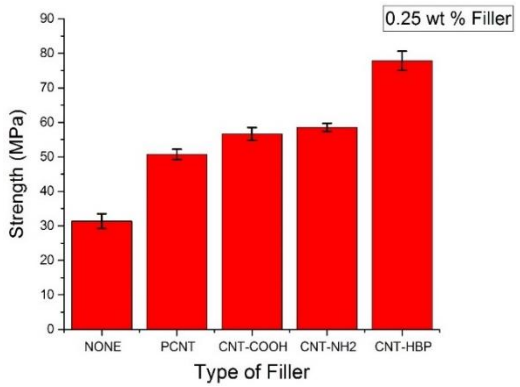

Figure 4.21 Strength of 0.25 weight % filler loading for (a) No filler (b) PCNT (c) CNT-COOH (d) CNT-NH_2 (e) CNT-HBP

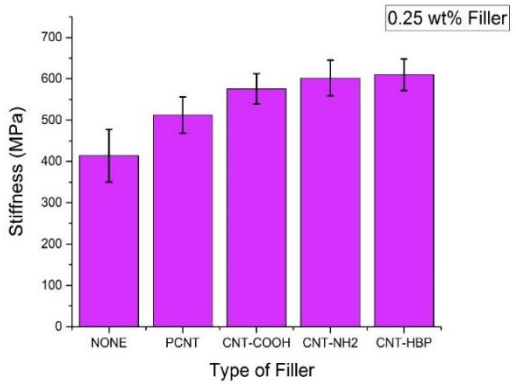

Figure 4.22 Stiffness of 0.25 weight % filler loading for (a) No filler (b) PCNT (c) CNT-COOH (d) CNT-NH_2 (e) CNT-HBP

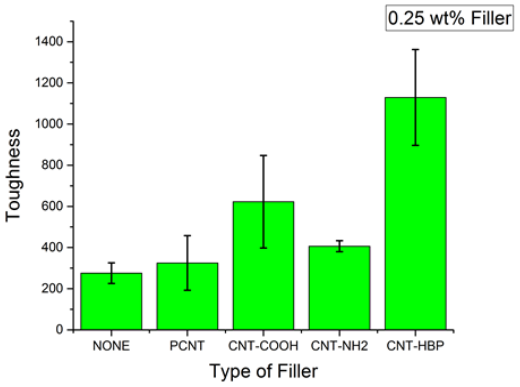

Figure 4.23 Toughness (in.lbf.in^{-3}) of 0.25 weight % filler loading for (a) No filler (b) PCNT (c) CNT-COOH (d) CNT-NH_2 (e) CNT-HBP

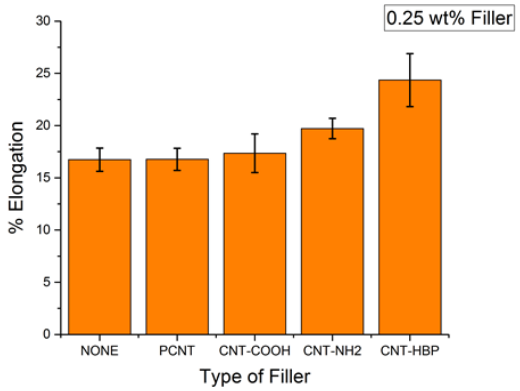

Figure 4.24 Elongation of 0.25 weight % filler loading for (a) No filler (b) PCNT (c) CNT-COOH (d) CNT-NH_2 (e) CNT-HBP

b) For filler loading of 0.5 weight%

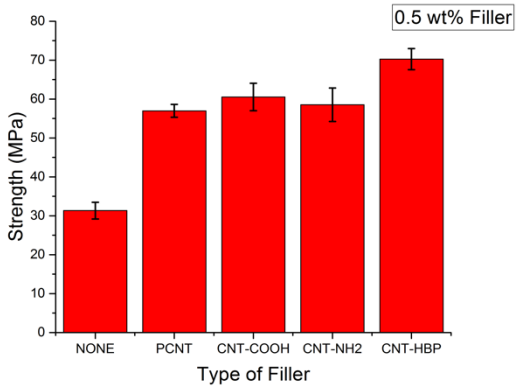

Figure 4.25 Strength of 0.5 weight % filler loading for (a) No filler (b) PCNT (c) CNT-COOH (d) CNT-NH_2 (e) CNT-HBP

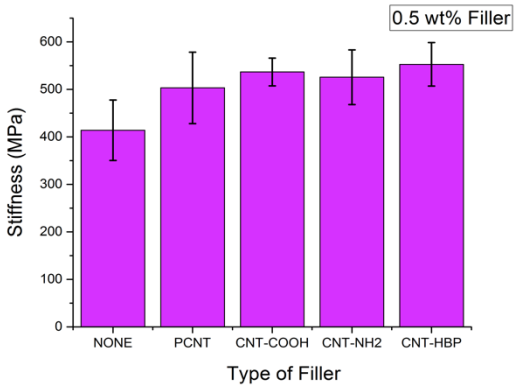

Figure 4.26 Stiffness of 0.5 weight % filler loading for (a) No filler (b) PCNT (c) CNT-COOH (d) CNT-NH_2 (e) CNT-HBP

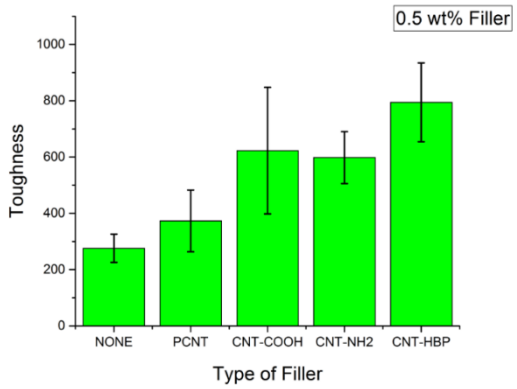

Figure 4.27 Toughness (in.lbf.in^{-3}) of 0.5 weight % filler loading for (a) No filler (b) PCNT (c) CNT-COOH (d) CNT-NH_2 (e) CNT-HBP

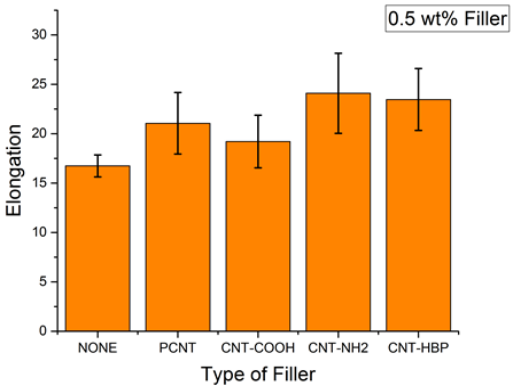

Figure 4.28 Elongation of 0.5 weight % filler loading for (a) No filler (b) PCNT (c) CNT-COOH (d) CNT-NH_2 (e) CNT-HBP

c) For filler loading of 1 weight%

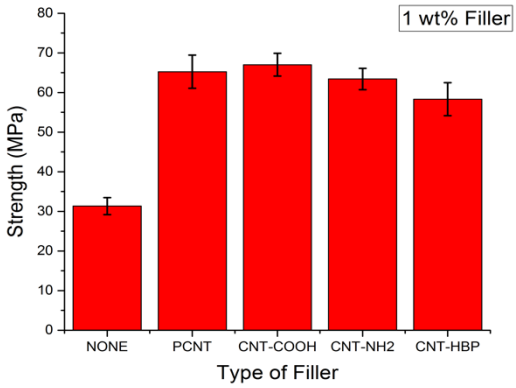

Figure 4.29 Strength of 1 weight % filler loading for (a) No filler (b) PCNT (c) CNT-COOH (d) CNT-NH_2 (e) CNT-HBP

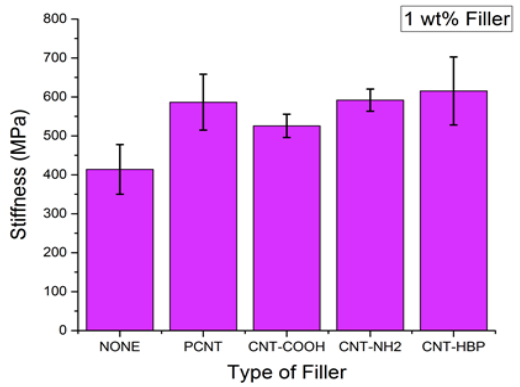

Figure 4.30 Stiffness of 1 weight % filler loading for (a) No filler (b) PCNT (c) CNT-COOH (d) CNT-NH_2 (e) CNT-HBP

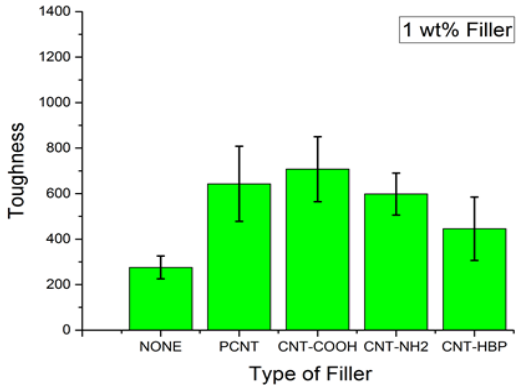

Figure 4.31 Toughness of (in.lbf.in^{-3}) 1 weight % filler loading for (a) No filler (b) PCNT (c) CNT-COOH (d) CNT-NH_2 (e) CNT-HBP

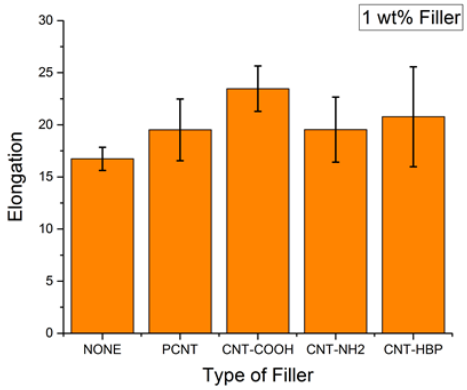

Figure 4.32 Elongation of 1 weight % filler loading for (a) No filler (b) PCNT (c) CNT-COOH (d) CNT-NH_2 (e) CNT-HBP

d) For filler loading of 1.5 weight%

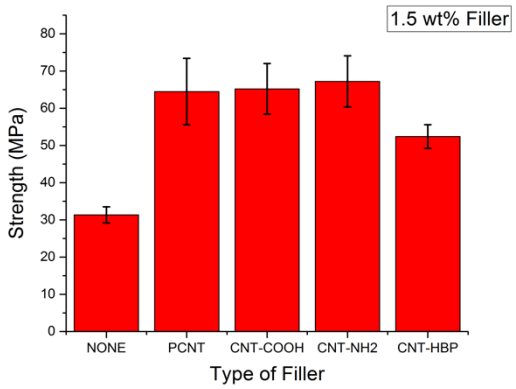

Figure 4.33 Strength of 1.5 weight % filler loading for (a) No filler (b) PCNT (c) CNT-COOH (d) CNT-NH_2 (e) CNT-HBP

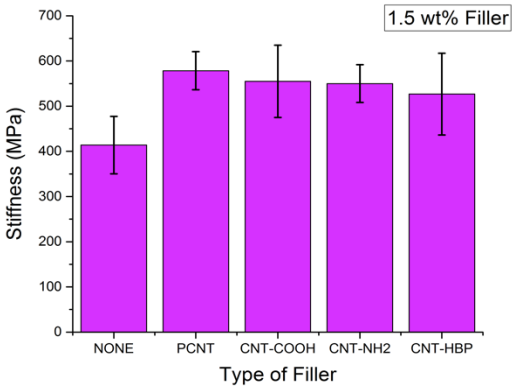

Figure 4.34 Stiffness of 1.5 weight % filler loading for (a) No filler (b) PCNT (c) CNT-COOH (d) CNT-NH_2 (e) CNT-HBP

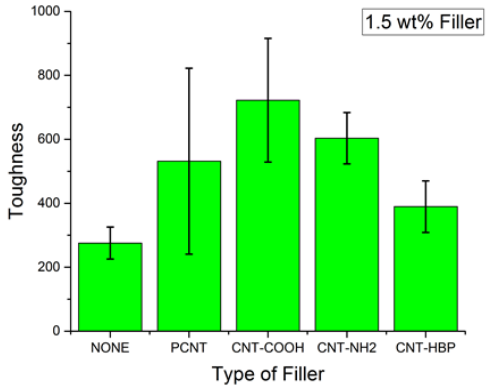

Figure 4.35 Toughness (in.lbf.in^{-3}) of 1.5 weight % filler loading for (a) No filler (b) PCNT (c) CNT-COOH (d) CNT-NH_2 (e) CNT-HBP

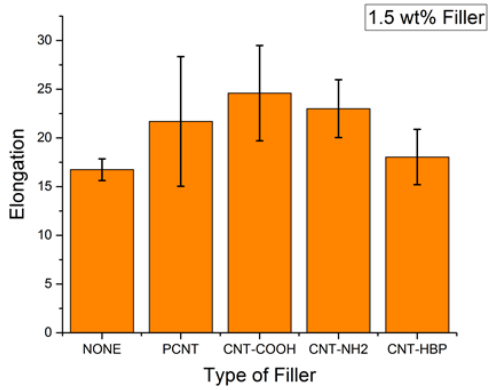

Figure 4.36 Elongation of 1.5 weight % filler loading for (a) No filler (b) PCNT (c) CNT-COOH (d) CNT-NH_2 (e) CNT-HBP

e) For filler loading of 2 weight%

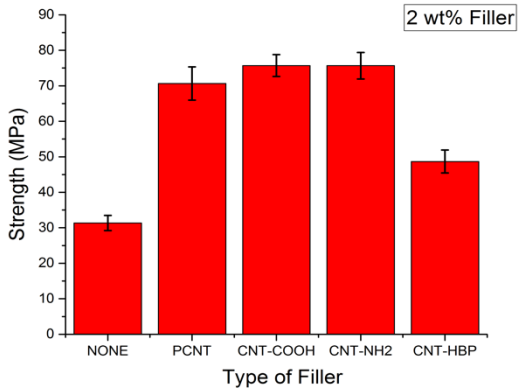

Figure 4.37 Strength of 2 weight % filler loading for (a) No filler (b) PCNT (c) CNT-COOH (d) CNT-NH_2 (e) CNT-HBP

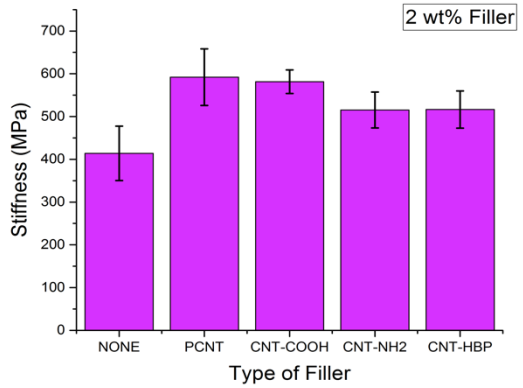

Figure 4.38 Stiffness of 2 weight % filler loading for (a) No filler (b) PCNT (c) CNT-COOH (d) CNT-NH_2 (e) CNT-HBP

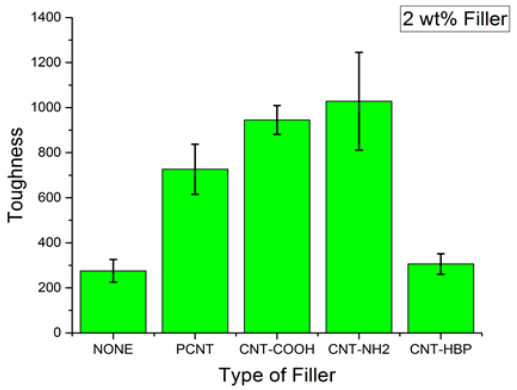

Figure 4.39 Toughness (in.lbf.in^{-3}) of 2 weight % filler loading for (a) No filler (b) PCNT (c) CNT-COOH (d) CNT-NH_2 (e) CNT-HBP

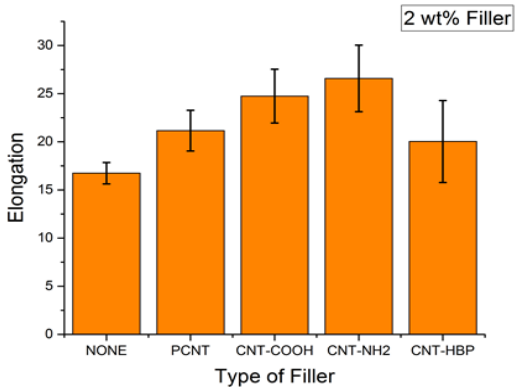

Figure 4.40 Elongation of 2 weight % filler loading for (a) No filler (b) PCNT (c) CNT-COOH (d) CNT-NH_2 (e) CNT-HBP

Property	0.25 wt% CNT-HBP	0.5 wt% CNT-HBP
Strength	310 %	188 %
Stiffness	47 %	34 %
Toughness	148 %	124 %
Elongation	46 %	44 %

Table 4-5 Percentage enhancement of properties.

4.6.2 Tensile Test Analysis

a) Strength Trend

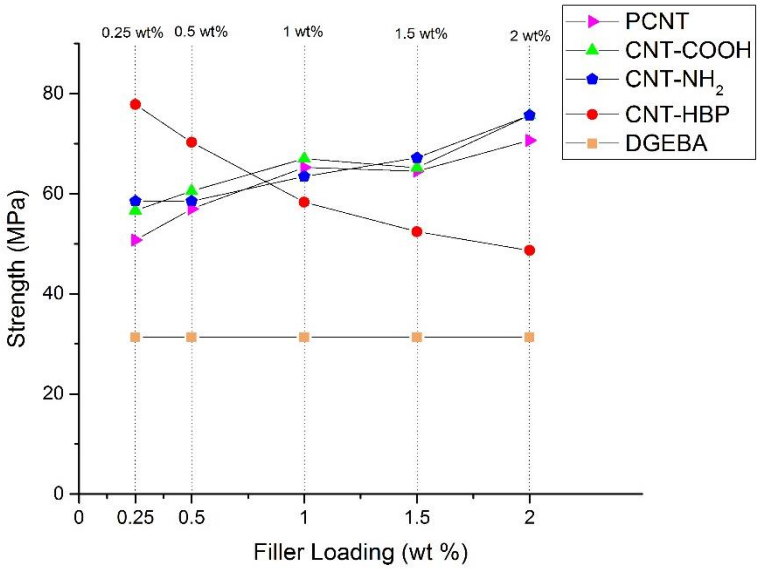

Figure 4.41 Strength trend for (a) No filler (b) PCNT (c) CNT-COOH (d) CNT-NH_2 (e) CNT-HBP

1. For 0.25 wt% and 0.5 wt% filler loading levels (by weight) the strength of the composite with CNT-HBP as the nanofiller is significantly large when compared to other types of fillers. This proves that Roding architecture of the filler increases the strength.
2. But for loading levels of 1, 1.5 wt% and 2 wt%, the strength decreases when CNT-HBP is used. This is because of following three reasons:

i. As the loading (weight %) of CNT-HBP increases the amount of HBP and CNT in the sample increases. This means that there are more chances for agglomeration (Difficulty of manually achieving homogeneous dispersion increases) which can be due to either attraction forces between CNTs or because of viscous HBP bound to CNT surface.

ii. As the filler loading level increases, the chance of agglomerate formation also increases due to manual mixing of samples. Bubbles that are invisible to the naked eye can be the reason for low stiffness.

iii. Finally as filler loading level increases, the amount of filler in the matrix increases, and so does the solvent used to disperse the filler into epoxy. 'Roding' nanofiller (CNT-HBP) was first dispersed in acetone before introducing it into epoxy matrix. The mixture was then heated till acetone gets evaporated. Bubbles can also be due to traces of acetone left on the filler surface, which evaporates during hot cast and curing process.

b) Stiffness Trend

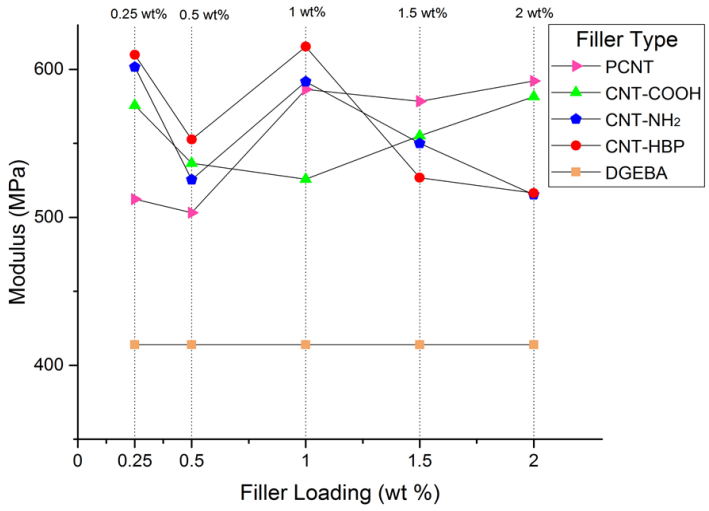

Figure 4.42 Stiffness trend for (a) No filler (b) PCNT (c) CNT-COOH (d) CNT-NH_2 (e) CNT-HBP

1. For 0.25 wt%, 0.5 wt%, 1 wt% filler loading level, the stiffness increases when the filler is CNT-HBP. This proves that 'Roding' architecture of filler increases the stiffness.
2. Stiffness decreases for 1.5 and 2 wt% loading levels when CNT-HBP is the filler. This decrease can again be attributed to the three reasons stated in the above section.

c) Toughness Trend

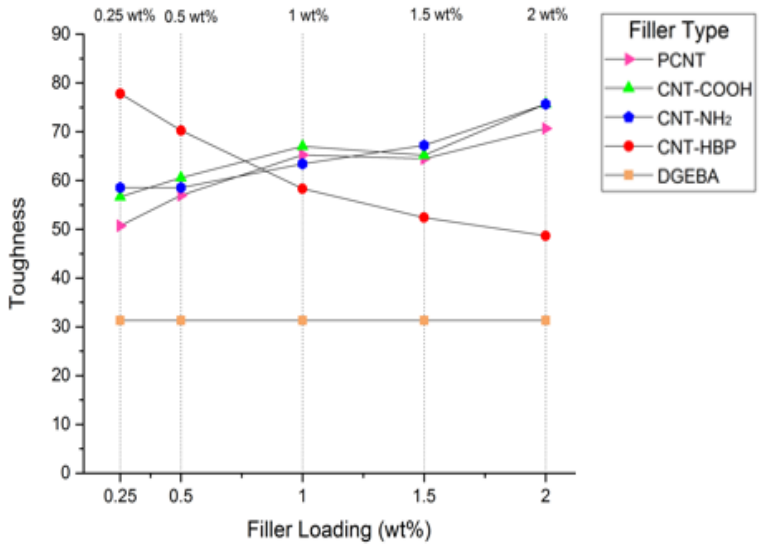

Figure 4.43 Toughness trend for (a) No filler (b) PCNT (c) CNT-COOH (d) CNT-NH_2 (e) CNT-HBP

1. Toughness increases for epoxy composites with CNT-HBP filler at 0.25 wt% and 0.5 wt%. This proves that the Roding hybrid nanofillers increase toughness.
2. As the trend shows, toughness decreases with increase in the filler loading. This is because of more aggloramation of filler and destruction of epoxy matrix properties due to solvent used to disperse the filler.

d) Elongation Trend

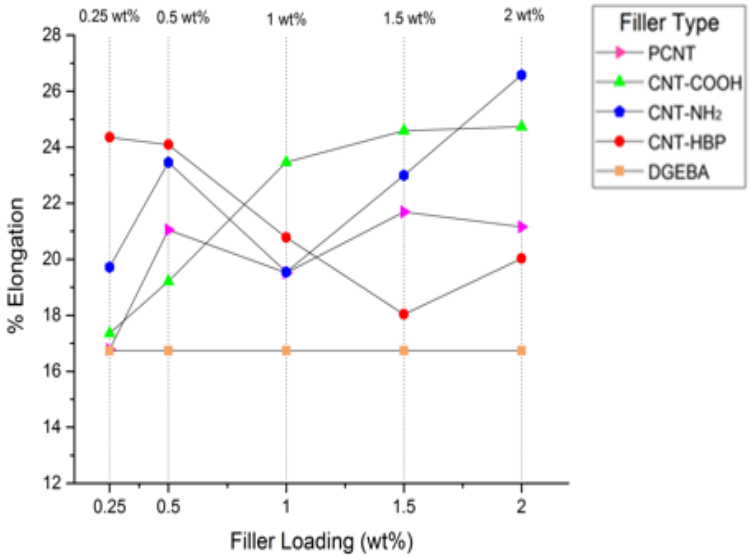

Figure 4.44 Elongation trend for (a) No filler (b) PCNT (c) CNT-COOH (d) CNT-NH_2 (e) CNT-HBP

1. Elongation increases for epoxy composites with CNT-HBP filler at 0.25 wt% and 0.5 wt%. This proves that the Roding hybrid nanofillers increase toughness.
2. As the trend indicates, toughness of the nanocomposite decreases with increase in the filler loading. This is because of more agglomeration of filler at higher loadings and destruction of epoxy matrix properties due to acetone which was used to disperse the filler.

e) *Tensile test results summary:* Observing the above reported percentage increase in mechanical properties, we can conclude that:

1. There is a high need for the optimization of the filler to matrix ratio. Though increasing filler loading is beneficial (as shown in the trends), it remains so only till a certain extent. Embedding too much filler into the matrix can potentially make it stiff and impractical for mass production (in terms of cost and effort). Thus, a compromise between filler loading percentage and mechanical performance of the

nanocomposite needs to be drawn while keeping in mind the constraint of limitations of cost.

2. Another important factor that needs to be kept in mind is the interaction between the filler and the matrix. When fillers with 'Roding' architecture are used there is a strong covalent interaction between the filler and the matrix. This is beneficial over physical blending of individual nanofillers into the matrix as physical blending may potentially disrupt the structure of the matrix. This disadvantage is overcome when fillers with 'Roding' architecture are used because the covalent bonding between the filler and matrix polymer ensures that intactness of intrinsic matrix structure.
3. Keeping in mind the manufacturing amenability of commercial nanocomposites, the filler loading level was limited to 2 weight % in all the nanocomposite samples.

4.7 Field Emission Scanning Electron Microscopy

Field Emission Scanning Electron Microscope uses electrons to scan the sample in a zig-zag manner. It has the capability to scan samples from sizes in nanoscale to microscale. The electrons produced by the field emission source are accelerated in a high electrical field gradient. According to the object being analyzed, the angle and voltage of the electrons are controlled. As soon as the incident electrons touch the surface of the sample, secondary electrons are emitted from its surface. These electrons are then captured by the detector and image processing is performed, which is displayed on the screen.

The cured epoxy with various compositions are cut into small, square like pieces and their surfaces are cleaned with pressurized air. Then the clean surfaces of the samples are

coated with platinum up to a thickness of ~2nm. Then they are placed on the sample holder and are inserted into the machine.

In this research, FE-SEM is performed on the broken cross sectional surfaces of the tensile samples, to study the fracture mechanism. SEM images also show the presence of agglomerates of in epoxy. These can be correlated with tensile results for better understanding of effect of filler on nanocomposite properties.

4.7.1 FE-SEM Results

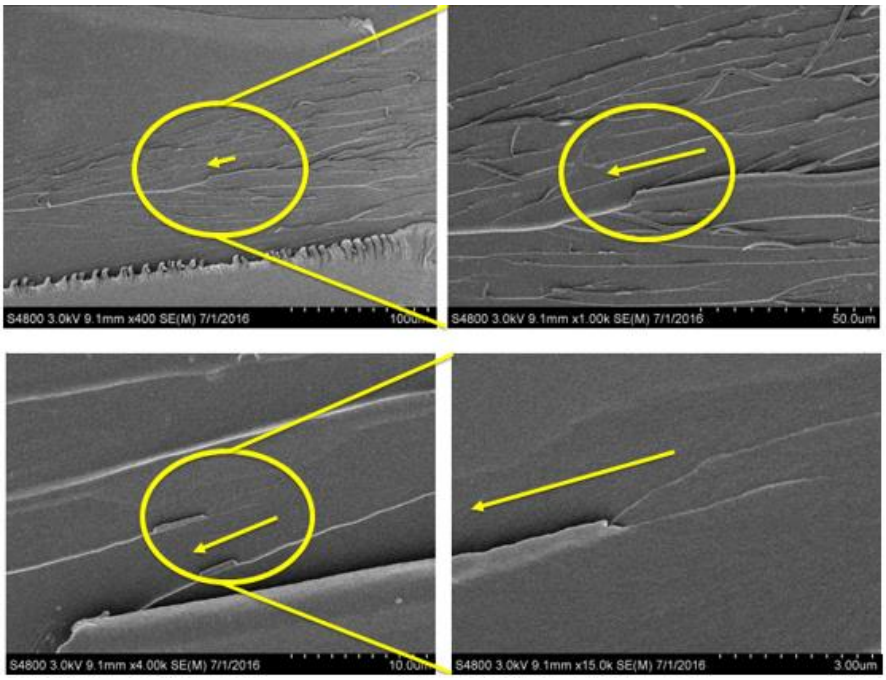

Figure 4.45 SEM of DGEBA sample

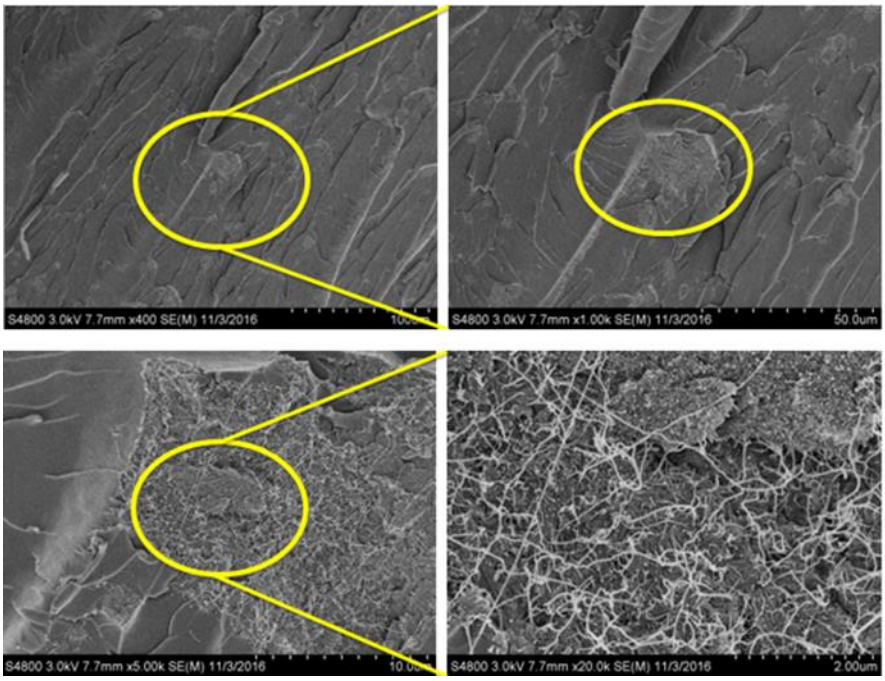

Figure 4.46 SEM of 1 wt% Pristine CNT & DGEBA

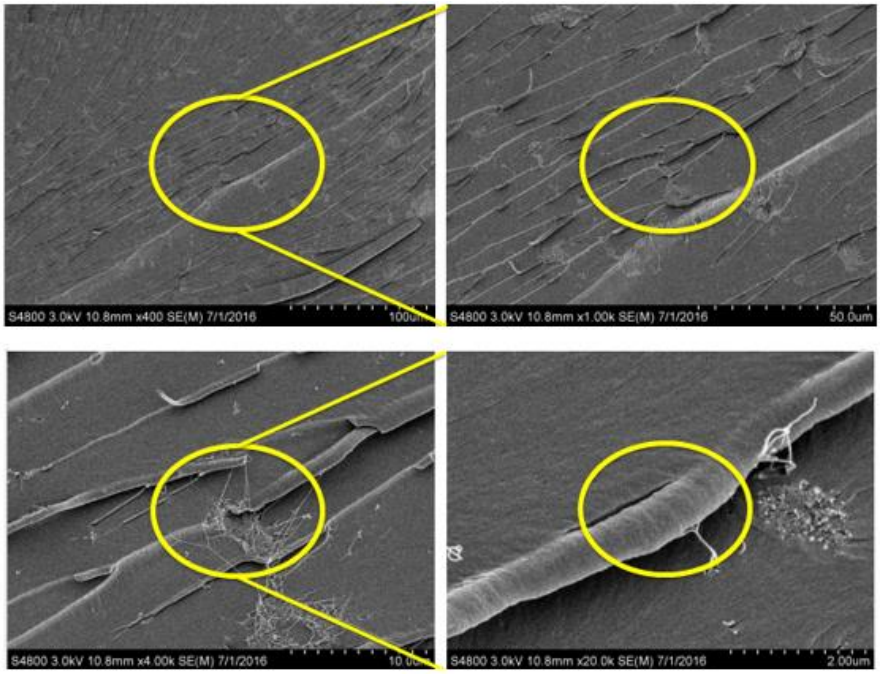

Figure 4.47 SEM of 1 wt% CNT-COOH & DGEBA

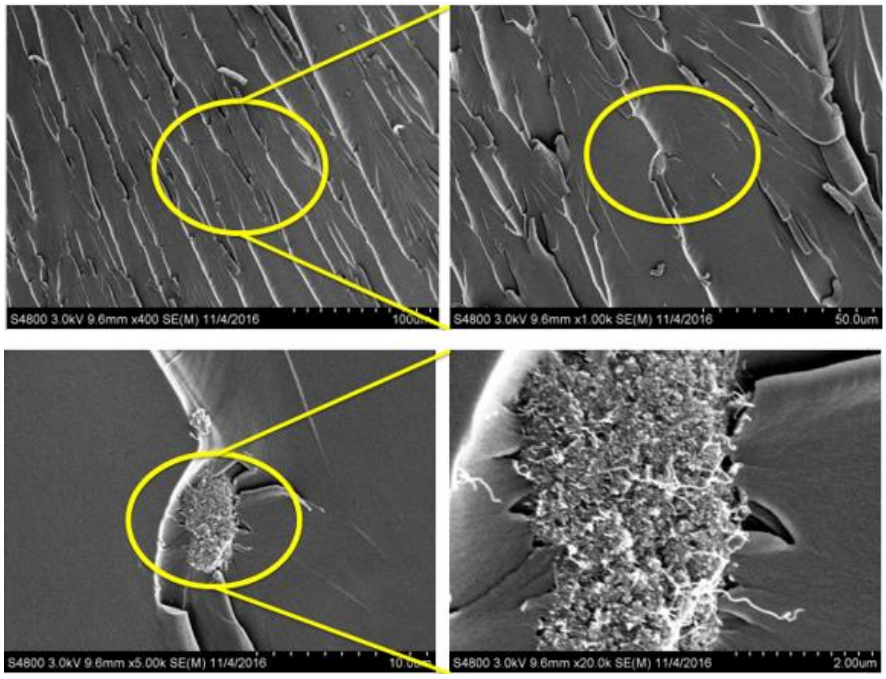

Figure 4.48 SEM of 1 wt% CNT-HBP & DGEBA

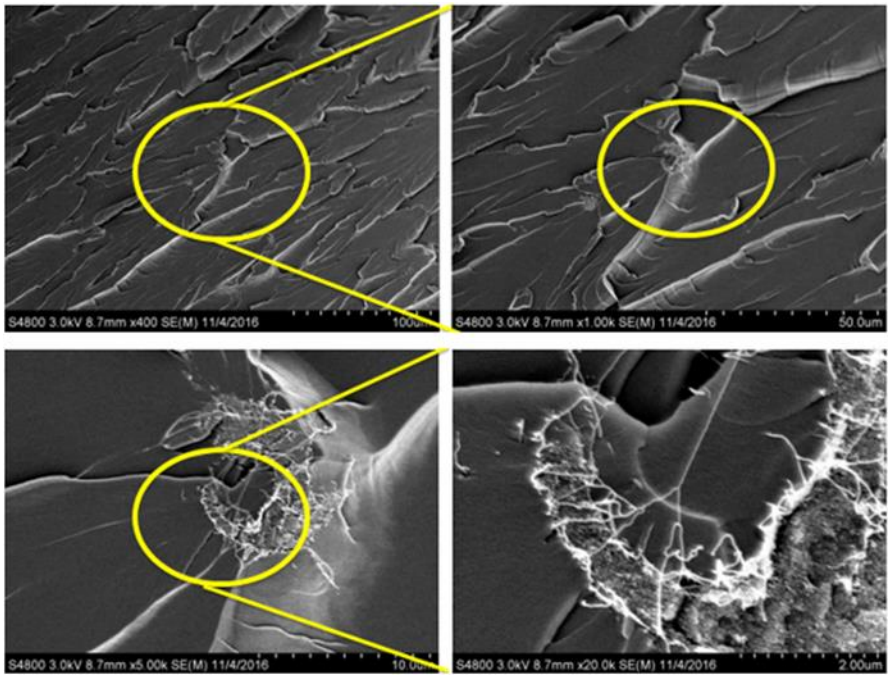

Figure 4.49 SEM of 0.25 wt% CNT-HBP & DGEBA

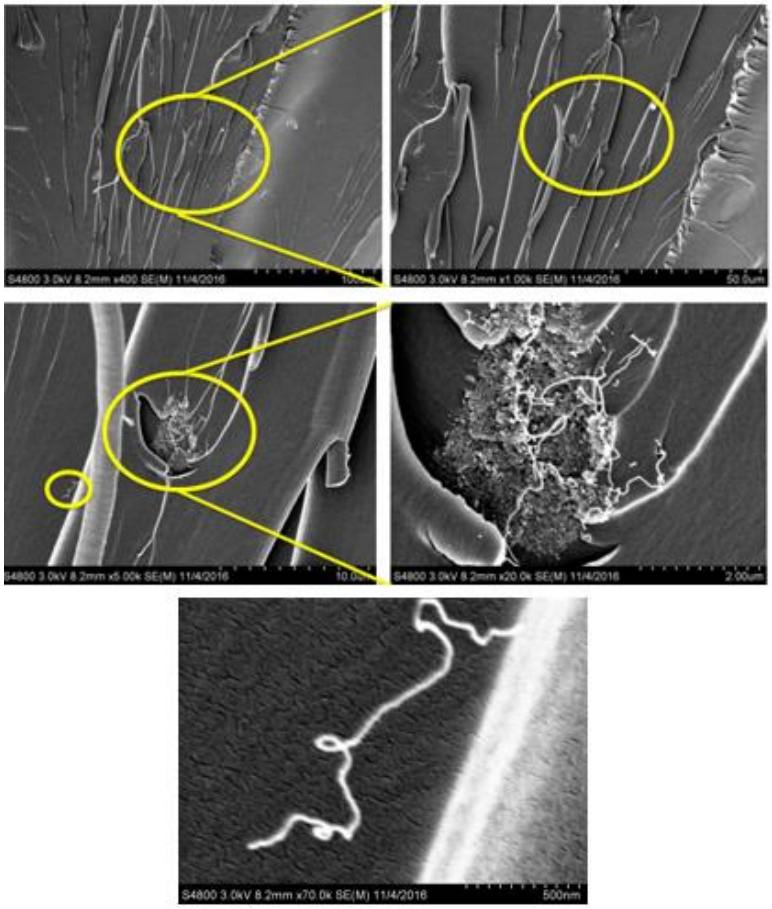

Figure 4.50 SEM of 0.5 wt% CNT-HBP & DGEBA

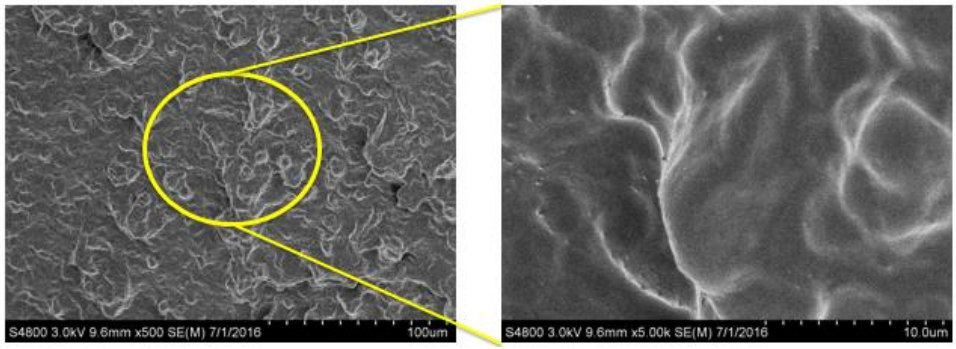

Figure 4.51 SEM of 5 wt% HBP & DGEBA

4.7.2 FE-SEM Analysis

a) *Interpretation of pure DGEBA Samples:* The fracture surface of the neat epoxy sample has a smooth surface showing brittle fracture of the sample. Direction of the crack propagation is represented by the arrow along the river line patterns (as shown in the figure)[96] . The results are as per expectation, as epoxies typically show brittle behavior.

b) *Interpretation for DGEBA and PCNT 1 wt. % sample:* The white highlighted regions in figure represent the agglomerates of CNTs. The pristine CNTs are embedded into the epoxy matrix as received. This bundling can be attributed to high aspect ratio of the nanotubes and also their inherent hydrophobicity. The agglomerates be seen as white 'patches' in the picture. When looked at the agglomeration at high resolution, it can be seen that they look like long lumps. Clearly, uniform dispersion is not achieved in the pristine CNT-DGEBA sample, explaining the poor mechanical properties. Another reason for low mechanical properties can be attributed to the negligible interaction between CNTs and the epoxy matrix, which in turn hinders the load transfer efficiency.

c) *Interpretation for DGEBA and CNT-COOH 1 wt. % sample:* When compared with the pristine CNT-DGEBA sample, the distribution of CNT-COOH in the matrix is highly uniform. This can be ascribed to the

chemical functionalization of CNTs, which improves the compatibility between the nanotubes and the epoxy matrix.

d) *Interpretation of the CNT-HBP samples:* The first observation that is very evident from the images, is the homogeneous filler distribution in the sample. This dispersion not only boosts the compatibility, but also enhances the load transfer between the nanofiller and the matrix. As seen in the pictures, pull out of CNTs is at a minimum showing excellent binding between the CNT and epoxy matrix. This leads to enhanced compatibility (may be due to chemical bond) and load transfer from matrix to filler. This is the reason behind high mechanical property values obtained. Also by examining the surface of the fractured sample, striations can be seen, showing ductile nature of the fracture. Thus, nanofillers with 'Roding' architecture can increase the ductility of the epoxy matrix. In order to reconfirm the above interpretations, the SEM was performed on the surfaces of the nanocomposites which displayed high mechanical properties. Both 0.5 wt. % and 0.25 wt. % CNT-HBP filler showed enhanced dispersion and increasing ductility of fracture. This explains their high values of mechanical properties.

e) *Interpretation for HBP-DGEBA 5 wt% sample:* The surface of the sample is very rough and is filed with striations clearly indicating the ductile nature of the fracture. It can thus be interpreted that HBP induces toughness into brittle thermoset matrices[33].

4.8 Soxhlet Extraction

It is simplest experiment for solid-liquid extraction. It is used for separating the solvent from the solid sample by washing the sample with the same solvent. Because of difference between the sample solubility's, one species is dissolved while the other remains intact.

As stated earlier, nanofillers with 'Roding' architecture need to have the ability to cure the epoxy matrix apart from imparting triumvirate properties. This is in fact, one of the main reasons for selecting hyperbranched polymers having amine and hydroxyl terminal functional groups. The two functional groups, can potentially cure the DGEBA epoxy by epoxide ring opening. In order to prove the possibility of curing reaction between HBP and DGEBA epoxy, soxhlet extraction was performed. According to stoichiometric calculations, ($x/2$) g of HBP should be able to completely cure (x) g of epoxy. But when both were mixed following the calculated ratio, only partial curing was achieved. The main reasons behind this can either be the pseudo nature of HBP generations (which makes it difficult to estimate exactly number of functional groups present in a particular weight of HBP) or steric hindrance between similar functional groups (this makes it impossible for all the 32 functional groups present on the terminal ends of HBP to react and cure the epoxy). So it was deduced that an extra weight (Δx) g of HBP needs to be added to achieve 100 % curing of the epoxy matrix. In order to prove this hypothesis, as an initial attempt HBP-NH_2 and DGEBA epoxy are mixed together in varying ratios and are allowed to cure for 2 h at 100 ^{0}C, before they are placed in the thimble. Their weights were monitored to analyze the cure reaction. DMF was taken as the solvent to perform the soxhlet extraction,

the reason being its capability to dissolve HBP easily. Naturally, unreacted HBP (the extra amount left after completely curing the epoxy) will be washed away, leaving behind just the cured sample.

The extraction was performed twice to get a result that is quantitatively accurate. The time taken for one wash was approximately 7 minutes and each sample was washed 300 times. Here the 'cured sample' refers to the HBP-NH_2 and DGEBA mixture, which was allowed to cure. Four different HBP: epoxy ratios were considered in this experiment. The different sample compositions are represented in the table.

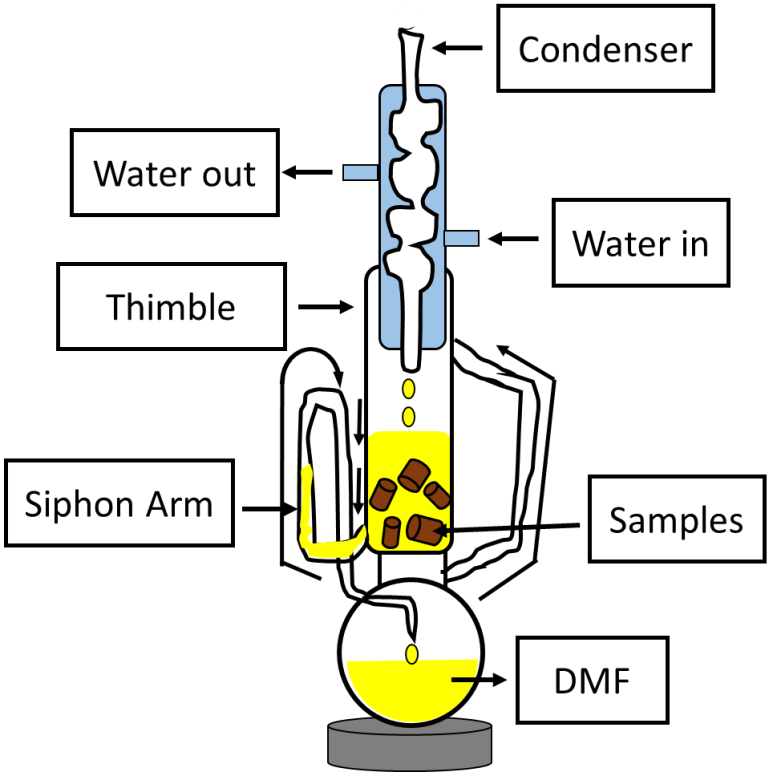

Figure 4.52 Soxhlet extraction concept

4.8.1 Soxhlet Extraction Results:

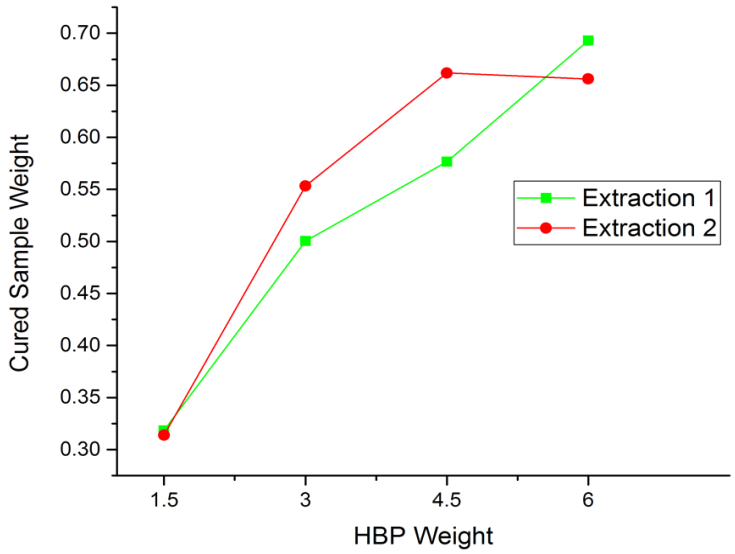

Figure 4.53 Weight of cured sample vs HBP

4.8.2 Soxhlet Extraction Analysis

From the results it can be seen that the weight of the cured sample increases as the amount of HBP increases. Increasing trend proves the curing between HBP and Epoxy. When extraction was performed only on HBP, the complete sample was washed away as can be seen from the results. As we have more amine groups that can react with the epoxide rings in the epoxy, the cured sample weight increases as the weight of HBP increases. This shows that it is always good to have abundant amine groups for the coupling to take place. But that increase the HBP content which will in turn keep turning the hybrid nanofiller amorphous. So this ratio should be controlled and optimized before commercial use of the hybrid 'Roding' nanofiller produced in this research.

After calculating exact stoichiometric ratio of HBP needed to cure the epoxy ($x + \Delta x$) g, it can be coupled with CNT using coupling reactions mentioned above to achieve

'Roding' nanofiller that can potentially cure the epoxy matrix. This determination needs extensive repetitions of iterations and techniques like DSC & TGA. This step is considered for future work.

4.9 Attenuated Total Reflectance Technique

This technique when combined with IR spectroscopy is very helpful in analyzing solid samples without destroying them. The experimental process of ATR is much similar to FTIR where an IR beam is focused into a crystal with high refractive index (like diamond), and the internally reflected light causes an evanescent wave that goes through the sample. The sample absorbs this energy, thus attenuating the evanescent wave. The beam after attenuation by the sample is again reflected back into the crystal which directs it into a spectrometer, which records the IR spectra.

In order to figure out the hypothesis that we can use HBP-NH_2 to cure the epoxy, the cured samples, obtained after Soxhlet extraction were cut into thin slices and ATR was performed.

4.9.1 ATR Results

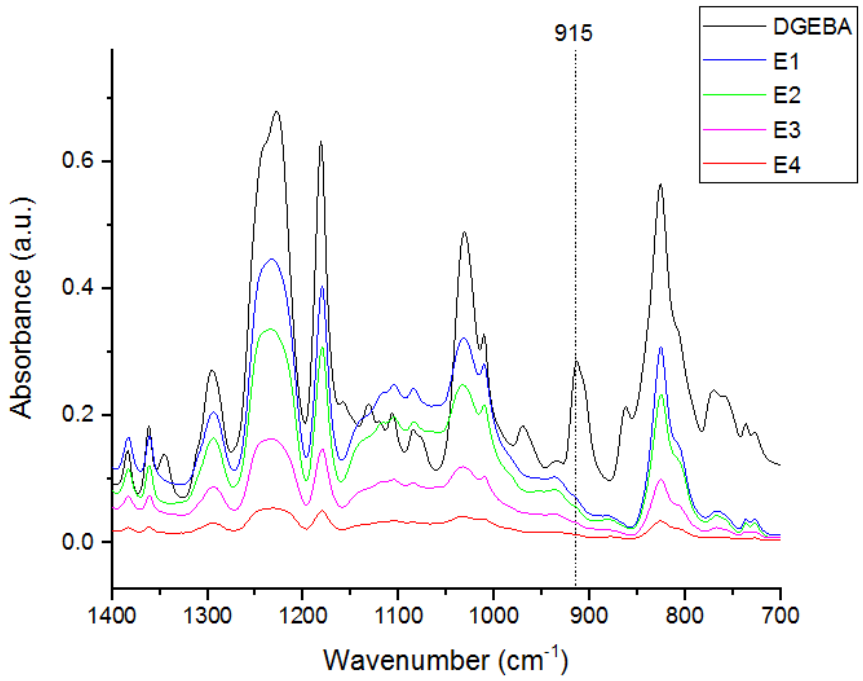

Figure 4.54 ATR result of (a) Pure epoxy-DGEBA (b) E1 (c) E2 (d) E3 (e) E4

4.9.2 ATR Analysis

These samples are obtained after performing soxhlet extraction meaning, there is no excess HBP present. Only the cured epoxy remains and unreacted HBP is washed away. In order to verify this, spectra of ATR samples obtained after extraction were compared to ATR of pure epoxy. The peak around 915 cm^{-1} corresponds to epoxide groups[98]. During the curing of epoxy, these epoxide rings are opened to facilitate crosslinking. The results of samples E1, E2, E3, E4 which are obtained after soxhlet extraction clearly show that decrease at ~ 915cm^{-1} proving that the HBP has cured the epoxy.

5 CONCLUSIONS AND FUTURE WORK

5.1 Conclusions

This thesis addressed the following there points:

a) The proposed research hypothesis was successfully tested for nanoscale reinforcements. FTIR and Raman spectroscopy results proved that the pristine CNTs have been functioned. The covalent bond between the 'Rod' element and 'Dampening' element was analyzed through FTIR & XPS techniques, showing the success of the coupling technique used. The structure of the hybrid 'Roding' nanofillers was studied using XRD and it showed that the covalent coupling of HBP with CNT, has turned the crystalline CNT into a semicrystalline nanofiller. TGA was used to estimate the thermal stability of the hybrid 'Roding' nanofillers and it was found that the 'Roding' nanofillers are very stable in comparison with pure HBP.

b) Overall, strength improvement of 310 %, stiffness improvement of 47% and toughness improvement of 148% was observed in the nanocomposite with 0.25 wt% of 'Roding' nanofillers compared to neat DGEBA. Tensile results show that incorporating hybrid nanofillers with 'Roding' architecture into the epoxy matrix improves the strength, stiffness and toughness significantly. The FE-SEM results show how nanofillers with 'Roding' architecture effects the crack propagation through the thermoset matrix.

c) It was also observed that appropriate selection of coupling chemistry (e.g. primary amine in this case) for the designed 'Roding' architecture may lead to elimination

of crosslinking agent that not only saves cost but also provides enhanced interfacial compatibility of the 'Roding' reinforcement with the matrix. The hypothesis that the epoxy can be cured with epoxy was verified through the method of soxhlet extraction.

5.2 Future Work

As the success of 'Roding' architecture was explained through the results, there are many ways in which this research can be developed.

a) The 'Roding' architecture can be verified by substituting 'Rod' and 'Dampening' elements with some of the multiple options presented in above sections.
b) The ratio of HBP grafted onto CNT can be quantitatively optimized and the influence of this ratio on improving the toughness of the matrix can be studied.
c) Optimization of the interfacial bonds between 'Roding' nanofillers and matrix and influence of their orientation on the mechanical properties of the nanocomposite is under study to attain controlled and predictable performance metrics.
d) The surface of the 'Roding' nanofiller can be visualized though advanced microscopy techniques like TEM and the possibility of controlling the position of HBP attachment onto the CNT surface can be investigated.
e) While the study tested the research hypothesis using thermoset matrices, similar studies can be conducted on thermoplastics materials multiple matrices like thermoplastic, metal, foams, bioplastic etc. which provide enhanced design and manufacturing flexibility.

f) As this research showed the influence of hybrid nanoscale fillers with ‘Roding’ architecture, the sample concept can be applied at micro and macroscales and the possibility of translation of material properties vs the scale of the filler and matrices can be studied.

g) The experimental results obtained by incorporating ‘Roding’ nanofillers into thermoset matrices can be verified using molecular dynamics simulations.

h) Influence of preparation methods of nanocomposites (like using a dissolver disc, shear intensive mechanical stirring, twin screw extruder, calendaring etc.) on their mechanical properties can be studied.

i) Study of magnetic and electrical properties of the nanocomposites with ‘Roding’ nanofillers can be done.

j) While the proposed ‘Roding’ architecture and its effect on triumvirate properties of composites is proven for nanoscale reinforcements, similar methodology may be employed for micro and macro scale reinforcements, which are prime drivers for large scale applications in current automotive sector.

k) While the field of ‘Roding’ architecture and related concepts are attracting increased attention, the discovery of more such materials necessitate accelerated innovations via molecular dynamics, genetic-algorithm-based theories and perhaps materials informatics.

l) While the study provided a feasible understanding of custom functionalization promoting curing of matrix, its fundamental investigation including stoichiometric ratio understanding and cure-kinetics is yet to be explored. Effect of nanofillers

with ‘Roding’ architecture on the curing kinetics of the epoxy can be studied in detail using characterization techniques like DSC.

m) The study provides a new concept architectural study using 1D materials. However, the concept can be extended to other nanoscale reinforcements such as 0D, 2D and/or 3D and can potentially have far-reaching impacts on the eventual performance metrics of the composites.

n) Controlled positioning of the nanoparticle and effects of entropy and enthalpy need to be explored.

o) Potential scalability and cost effective manufacturing techniques of synthesizing ‘Roding’ nano reinforcements can be analyzed.

p) Apart from ‘Roding’ architecture different other architectures, their possible synthesis and effect on matrix properties can be studied.

5.3 Broader Impact

Nanofillers with ‘Roding’ architecture are expected to influence the mechanical properties of any matrix into which they are incorporated. Though in this initial attempt ‘Roding’ architecture was proven via realizing the architecture at a nanoscale, the same can be translated into micro and macro scale to suit the mass production needs of the transportation industry. They have the potential to make the composite tougher, stronger and stiffer. The level of improvement in stiffness, strength and toughness is related to the percentage of the filler with ‘Roding’ architecture present in the composite. The catch here is not to restrict ourselves to a particular morphology but to explore the opportunity to

customize the composite morphology, which has the potential to revolutionize the very basics of engineering and materials, as we know them.

The goal of the research is to elucidate the concept that one can design his own composite to fit targeted application by controlling the morphology and composition of the composite materials. This concept is proved by taking one-application namely automotive body structures and by developing composite material solutions that are capable of satisfying all the requirements of the same. Just by considering one application, we have developed many viable options by controlling the material morphology. This concept when translated into large scale has the potential to transform the transportation and material industry and act as a portal of possibilities and challenges for material customization.

REFERENCES

1. Porter, B.; Blaxill, H.; Jariri, N., A Study of Potential Fuel Economy Technologies to Achieve CAFE 2025 Regulations using Fleet Simulation Modeling Software. *SAE International Journal of Alternative Powertrains* ***2015,*** *4* (2015-01-1683), 352-362.
2. Strother, C. E.; Woolley, R. L.; James, M. B. *A comparison between NHTSA crash test data and CRASH3 frontal stiffness coefficients*; 0148-7191; SAE Technical Paper: 1990.
3. Malen, D. E. *Fundamentals of automobile body structure design*; SAE Technical Paper: 2011.
4. Kickelbick, G., *Hybrid materials: synthesis, characterization, and applications*. John Wiley & Sons: 2007.
5. Ray, S. S.; Bousmina, M., *Polymer nanocomposites and their applications*. American Scientific: 2006.
6. Uyama, H.; Kuwabara, M.; Tsujimoto, T.; Nakano, M.; Usuki, A.; Kobayashi, S., Green nanocomposites from renewable resources: plant oil-clay hybrid materials. *Chemistry of Materials* ***2003,*** *15* (13), 2492-2494.
7. Sanchez, C.; Soler-Illia, G. d. A.; Ribot, F.; Lalot, T.; Mayer, C.; Cabuil, V., Designed hybrid organic-inorganic nanocomposites from functional nanobuilding blocks. *Chemistry of Materials* ***2001,*** *13* (10), 3061-3083.
8. Kaushik, A.; Kumar, R.; Arya, S. K.; Nair, M.; Malhotra, B.; Bhansali, S., Organic–inorganic hybrid nanocomposite-based gas sensors for environmental monitoring. *Chemical reviews* ***2015,*** *115* (11), 4571-4606.
9. Bae, B.-S.; Eo, Y.-J.; Lee, T.-H.; Kim, J.-H., Inorganic/organic hybrid oligomer and nano hybrid polymer for use in optical devices and displays, and process for preparing the same. Google Patents: 2005.
10. Patel, V.; Mahajan, Y., Polymer nanocomposites: emerging growth driver for the global automotive industry. In *Handbook of Polymernanocomposites. Processing, Performance and Application*, Springer: 2014; pp 511-538.
11. Grijpma, D. W.; Hou, Q.; Feijen, J., Preparation of biodegradable networks by photo-crosslinking lactide, ε-caprolactone and trimethylene carbonate-based oligomers functionalized with fumaric acid monoethyl ester. *Biomaterials* ***2005,*** *26* (16), 2795-2802.
12. Lacour, S., Emerging Questions for Emerging Technologies: Is There a Law for the Nano? In *Nanomaterials: A Danger or a Promise?*, Springer: 2013; pp 357-378.
13. Singh, R.; Lillard, J. W., Nanoparticle-based targeted drug delivery. *Experimental and molecular pathology* ***2009,*** *86* (3), 215-223.
14. Couvreur, P., Polyalkylcyanoacrylates as colloidal drug carriers. *Critical reviews in therapeutic drug carrier systems* ***1987,*** *5* (1), 1-20.
15. LewisOscar, F.; Vismaya, S.; Arunkumar, M.; Thajuddin, N.; Dhanasekaran, D.; Nithya, C., Algal Nanoparticles: Synthesis and Biotechnological Potentials. ***2016***.

16. Pérez-Juste, J.; Pastoriza-Santos, I.; Liz-Marzán, L. M.; Mulvaney, P., Gold nanorods: synthesis, characterization and applications. *Coordination Chemistry Reviews* ***2005,*** *249* (17), 1870-1901.
17. Rihtnesberg, D. B.; Almqvist, S.; Wang, Q.; Sugunan, A.; Yang, X.; Toprak, M.; Besharat, Z.; Göthelid, M. In *ZnO nanorods/nanoflowers and their applications*, 4th IEEE International Nanoelectronics Conference, INEC 2011, 21 June 2011 through 24 June 2011, Tao-Yuan, 2011.
18. Liu, Y.; Hu, W.; Wang, X.; Long, C.; Zhang, J.; Zhu, D.; Tang, D.; Xie, S., Carbon nanorods. *Chemical Physics Letters* ***2000,*** *331* (1), 31-34.
19. Luo, J.; Liu, C.; Yang, S.; Cao, Y., Hybrid solar cells based on blends of poly (3-hexylthiophene) and surface dye-modified, ultrathin linear-and branched-TiO 2 nanorods. *Solar energy materials and solar cells* ***2010,*** *94* (3), 501-508.
20. Ajayan, P. M.; Zhou, O. Z., Applications of carbon nanotubes. In *Carbon nanotubes*, Springer: 2001; pp 391-425.
21. Rinzler, A.; Hafner, J.; Nikolaev, P.; Lou, L., Unraveling nanotubes: field emission from an atomic wire. *Science* ***1995,*** *269* (5230), 1550.
22. Odom, T. W.; Huang, J.-L.; Kim, P.; Lieber, C. M., Atomic structure and electronic properties of single-walled carbon nanotubes. *Nature* ***1998,*** *391* (6662), 62-64.
23. Li, C.; Chou, T.-W., A structural mechanics approach for the analysis of carbon nanotubes. *International Journal of Solids and Structures* ***2003,*** *40* (10), 2487-2499.
24. Wong, E. W.; Sheehan, P. E.; Lieber, C. M., Nanobeam mechanics: elasticity, strength, and toughness of nanorods and nanotubes. *Science* ***1997,*** *277* (5334), 1971-1975.
25. Tjong, S. C., Structural and mechanical properties of polymer nanocomposites. *Materials Science and Engineering: R: Reports* ***2006,*** *53* (3), 73-197.
26. Hernandez, E.; Goze, C.; Bernier, P.; Rubio, A., Elastic properties of C and B x C y N z composite nanotubes. *Physical Review Letters* ***1998,*** *80* (20), 4502.
27. Odom, T. W.; HUANG, J. L.; Lieber, C. M., Single‐Walled Carbon Nanotubes. *Annals of the New York Academy of Sciences* ***2002,*** *960* (1), 203-215.
28. Lau, K.-t.; Gu, C.; Hui, D., A critical review on nanotube and nanotube/nanoclay related polymer composite materials. *Composites Part B: Engineering* ***2006,*** *37* (6), 425-436.
29. Lau, K.-T.; Gu, C.; Gao, G.-H.; Ling, H.-y.; Reid, S. R., Stretching process of single-and multi-walled carbon nanotubes for nanocomposite applications. *Carbon* ***2004,*** *42* (2), 426-428.
30. Lau, K.-T.; Chipara, M.; Ling, H.-Y.; Hui, D., On the effective elastic moduli of carbon nanotubes for nanocomposite structures. *Composites Part B: Engineering* ***2004,*** *35* (2), 95-101.
31. Kim, J.-Y.; Ok, C.-Y.; Lee, S.-W.; Huh, W., Synthesis and characterization of aliphatic hyperbranched polyesters. *Polymer Korea* ***2005,*** *29* (6), 575-580.
32. Lee, J.; Yee, A., Role of inherent matrix toughness on fracture of glass bead filled epoxies. *Polymer* ***2000,*** *41* (23), 8375-8385.
33. Harani, H.; Fellahi, S.; Bakar, M., Toughening of epoxy resin using hydroxyl‐terminated polyesters. *Journal of Applied Polymer Science* ***1999,*** *71* (1), 29-38.

34. Roco, M.; Williams, R.; Alivisatos, P., Interagency Working Group in Nanoscience Engineering and Technology (IWGN) Workshop Report: Nanotechnology Research Directions; Vision for Nanotechnology R and D in the Next Decade, Published by Int. *Tech. Research Institutes, WTEC Division, Loyola College* ***1999***.
35. Misra, A.; Verdier, M.; Lu, Y.; Kung, H.; Mitchell, T.; Nastasi, M.; Embury, J., Structure and mechanical properties of Cu-X (X= Nb, Cr, Ni) nanolayered composites. *Scripta Materialia* ***1998,*** *39* (4), 555-560.
36. Gao, H.; Ji, B.; Jäger, I. L.; Arzt, E.; Fratzl, P., Materials become insensitive to flaws at nanoscale: lessons from nature. *Proceedings of the national Academy of Sciences* ***2003,*** *100* (10), 5597-5600.
37. Poole Jr, C. P.; Owens, F. J., *Introduction to nanotechnology*. John Wiley & Sons: 2003.
38. Sobolev, K.; Gutiérrez, M. F., How nanotechnology can change the concrete world. *American Ceramic Society Bulletin* ***2005,*** *84* (10), 14.
39. Han, K.; Embury, J.; Sims, J.; Campbell, L.; Schneider-Muntau, H.-J.; Pantsyrnyi, V.; Shikov, A.; Nikulin, A.; Vorobieva, A., The fabrication, properties and microstructure of Cu–Ag and Cu–Nb composite conductors. *Materials Science and Engineering: A* ***1999,*** *267* (1), 99-114.
40. Sajanlal, P. R.; Sreeprasad, T. S.; Samal, A. K.; Pradeep, T., Anisotropic nanomaterials: structure, growth, assembly, and functions. *Nano Reviews & Experiments* ***2011,*** *2*.
41. Gleiter, H., Nanostructured materials. *Advanced Materials* ***1992,*** *4* (7 - 8), 474-481.
42. Pal, S. L.; Jana, U.; Manna, P.; Mohanta, G.; Manavalan, R., Nanoparticle: An overview of preparation and characterization (2000-2010). ***2011***.
43. Levy, J.-C. S., *Magnetic Structures of 2D and 3D Nanoparticles: Properties and Applications*. CRC Press: 2016.
44. D'Elia, G.; Holsten, F., Kognitiv terapi har visat god effekt på panikångest. *LAKARTIDNINGEN* ***1998***, 4869-4873.
45. Fazelpour, M.; Shankar, P.; Summers, J. D. In *Developing Design Guidelines for Meso-scaled Periodic Cellular Material Structures under Shear Loading*, ASME 2016 International Design Engineering Technical Conferences and Computers and Information in Engineering Conference, ASME, Charlotte, NC, pp. DETC2016–59082, 2016.
46. Shankar, P.; Fazelpour, M.; Summers, J. In *An Energy-Based Approach for Design of Meso-Structures with High Shear Flexure*, International Design Engineering Technical Conferences and Computers and Information in Engineering Conference, 2013.
47. Yoder, M.; Satterfield, Z.; Fazelpour, M.; Summers, J. D.; Fadel, G. In *Numerical Methods for the Design of Meso-Structures: A Comparative Review*, ASME 2015 International Design Engineering Technical Conferences and Computers and Information in Engineering Conference, American Society of Mechanical Engineers: 2015; pp V02BT03A003-V02BT03A003.
48. Elghanian, R.; Storhoff, J. J.; Mucic, R. C.; Letsinger, R. L.; Mirkin, C. A., Selective colorimetric detection of polynucleotides based on the distance-dependent optical properties of gold nanoparticles. *Science* ***1997,*** *277* (5329), 1078-1081.

49. Petit, C.; Taleb, A.; Pileni, M., Cobalt nanosized particles organized in a 2D superlattice: synthesis, characterization, and magnetic properties. *The Journal of Physical Chemistry B* ***1999,*** *103* (11), 1805-1810.
50. Schmid, G.; Simon, U., Gold nanoparticles: assembly and electrical properties in 1–3 dimensions. *Chemical communications* ***2005,*** (6), 697-710.
51. Huang, X.; Jain, P. K.; El-Sayed, I. H.; El-Sayed, M. A., Gold nanoparticles: interesting optical properties and recent applications in cancer diagnostics and therapy. ***2007***.
52. Wang, C.; Yu, C., Detection of chemical pollutants in water using gold nanoparticles as sensors: a review. *Reviews in Analytical Chemistry* ***2013,*** *32* (1), 1-14.
53. Luo, X.; Morrin, A.; Killard, A. J.; Smyth, M. R., Application of nanoparticles in electrochemical sensors and biosensors. *Electroanalysis* ***2006,*** *18* (4), 319-326.
54. Miro, P.; Audiffred, M.; Heine, T., An atlas of two-dimensional materials. *Chemical Society Reviews* ***2014,*** *43* (18), 6537-6554.
55. Choi, B. G.; Yang, M. H.; Park, T. J.; Huh, Y. S.; Lee, S. Y.; Hong, W. H.; Park, H., Programmable peptide-directed two dimensional arrays of various nanoparticles on graphene sheets. *Nanoscale* ***2011,*** *3* (8), 3208-3213.
56. Horsford, W.; Backofen, W. In *Strength and Plasticity of Textured Materials*, Fundamentals of Deformation Processing: Proceedings of the 9th Sagamore Army Materials Research Conference, 1964; pp 259-298.
57. Xu, Z.; Li, Y.; Zhang, B.; Purkait, T.; Alb, A.; Mitchell, B. S.; Grayson, S. M.; Fink, M. J., Water-soluble PEGylated silicon nanoparticles and their assembly into swellable nanoparticle aggregates. *Journal of Nanoparticle Research* ***2015,*** *17* (1), 1-16.
58. Raja, S. N.; Olson, A. C.; Limaye, A.; Thorkelsson, K.; Luong, A.; Lin, L.; Ritchie, R. O.; Xu, T.; Alivisatos, A. P., Influence of three-dimensional nanoparticle branching on the Young's modulus of nanocomposites: Effect of interface orientation. *Proceedings of the National Academy of Sciences* ***2015,*** *112* (21), 6533-6538.
59. Knauert, S. T.; Douglas, J. F.; Starr, F. W., The effect of nanoparticle shape on polymer‐nanocomposite rheology and tensile strength. *Journal of Polymer Science Part B: Polymer Physics* ***2007,*** *45* (14), 1882-1897.
60. Lange, F.; Radford, K., Fracture energy of an epoxy composite system. *Journal of Materials Science* ***1971,*** *6* (9), 1197-1203.
61. Kim, G.-M.; Michler, G., Micromechanical deformation processes in toughened and particle-filled semicrystalline polymers: Part 1. Characterization of deformation processes in dependence on phase morphology. *Polymer* ***1998,*** *39* (23), 5689-5697.
62. Franco, M.; Mondragon, I.; Bucknall, C., Blends of epoxy resin with amine‐terminated polyoxypropylene elastomer: Morphology and properties. *Journal of applied polymer science* ***1999,*** *72* (3), 427-434.
63. Becker, O.; Varley, R.; Simon, G., Morphology, thermal relaxations and mechanical properties of layered silicate nanocomposites based upon high-functionality epoxy resins. *Polymer* ***2002,*** *43* (16), 4365-4373.
64. Wang, K.; Chen, L.; Wu, J.; Toh, M. L.; He, C.; Yee, A. F., Epoxy nanocomposites with highly exfoliated clay: mechanical properties and fracture mechanisms. *Macromolecules* ***2005,*** *38* (3), 788-800.

65. Gojny, F. H.; Wichmann, M. H.; Fiedler, B.; Schulte, K., Influence of different carbon nanotubes on the mechanical properties of epoxy matrix composites–a comparative study. *Composites Science and Technology* ***2005,*** *65* (15), 2300-2313.
66. Song, Y. S.; Youn, J. R., Influence of dispersion states of carbon nanotubes on physical properties of epoxy nanocomposites. *Carbon* ***2005,*** *43* (7), 1378-1385.
67. Kim, J. A.; Seong, D. G.; Kang, T. J.; Youn, J. R., Effects of surface modification on rheological and mechanical properties of CNT/epoxy composites. *Carbon* ***2006,*** *44* (10), 1898-1905.
68. Tang, W.; Santare, M. H.; Advani, S. G., Melt processing and mechanical property characterization of multi-walled carbon nanotube/high density polyethylene (MWNT/HDPE) composite films. *Carbon* ***2003,*** *41* (14), 2779-2785.
69. McNally, T.; Pötschke, P.; Halley, P.; Murphy, M.; Martin, D.; Bell, S. E.; Brennan, G. P.; Bein, D.; Lemoine, P.; Quinn, J. P., Polyethylene multiwalled carbon nanotube composites. *Polymer* ***2005,*** *46* (19), 8222-8232.
70. Shofner, M. L.; Khabashesku, V. N.; Barrera, E. V., Processing and mechanical properties of fluorinated single-wall carbon nanotube-polyethylene composites. *Chemistry of Materials* ***2006,*** *18* (4), 906-913.
71. Zhang, Q.; Rastogi, S.; Chen, D.; Lippits, D.; Lemstra, P. J., Low percolation threshold in single-walled carbon nanotube/high density polyethylene composites prepared by melt processing technique. *Carbon* ***2006,*** *44* (4), 778-785.
72. Mahfuz, H.; Adnan, A.; Rangari, V. K.; Jeelani, S., Manufacturing and characterization of carbon nanotube/polyethylene composites. *International Journal of Nanoscience* ***2005,*** *4* (01), 55-72.
73. Xiong, J.; Zheng, Z.; Qin, X.; Li, M.; Li, H.; Wang, X., The thermal and mechanical properties of a polyurethane/multi-walled carbon nanotube composite. *Carbon* ***2006,*** *44* (13), 2701-2707.
74. Mezzenga, R.; Månson, J., Thermo-mechanical properties of hyperbranched polymer modified epoxies. *Journal of materials science* ***2001,*** *36* (20), 4883-4891.
75. Parzuchowski, P. G.; Kiźlińska, M.; Rokicki, G., New hyperbranched polyether containing cyclic carbonate groups as a toughening agent for epoxy resin. *Polymer* ***2007,*** *48* (7), 1857-1865.
76. Xu, Y.; Gao, C.; Kong, H.; Yan, D.; Jin, Y. Z.; Watts, P. C., Growing multihydroxyl hyperbranched polymers on the surfaces of carbon nanotubes by in situ ring-opening polymerization. *Macromolecules* ***2004,*** *37* (24), 8846-8853.
77. Gao, C.; Muthukrishnan, S.; Li, W.; Yuan, J.; Xu, Y.; Müller, A. H., Linear and hyperbranched glycopolymer-functionalized carbon nanotubes: synthesis, kinetics, and characterization. *Macromolecules* ***2007,*** *40* (6), 1803-1815.
78. Hong, C.-Y.; You, Y.-Z.; Wu, D.; Liu, Y.; Pan, C.-Y., Multiwalled carbon nanotubes grafted with hyperbranched polymer shell via SCVP. *Macromolecules* ***2005,*** *38* (7), 2606-2611.
79. Wu, C.-S.; Liao, H.-T., Study on the preparation and characterization of biodegradable polylactide/multi-walled carbon nanotubes nanocomposites. *Polymer* ***2007,*** *48* (15), 4449-4458.

80. Yadav, S. K.; Mahapatra, S. S.; Cho, J. W., Synthesis of mechanically robust antimicrobial nanocomposites by click coupling of hyperbranched polyurethane and carbon nanotubes. *Polymer* ***2012,*** *53* (10), 2023-2031.
81. Yoon, J. T.; Jeong, Y. G.; Lee, S. C.; Min, B. G., Influences of poly (lactic acid)‐grafted carbon nanotube on thermal, mechanical, and electrical properties of poly (lactic acid). *Polymers for Advanced Technologies* ***2009,*** *20* (7), 631-638.
82. Liu, Y.; Wang, B.; Jing, X., Thermal properties of hyperbranched polyborate functionalized multiwall carbon nanotube/polybenzoxazine composites. *Polymer Composites* ***2011,*** *32* (9), 1352-1361.
83. Yang, K.; Gu, M., Fabrication, Morphology and Cure Behavior of Triethylenetetramine-Grafted Multiwalled Carbon Nanotube/Epoxy Nanocomposites. *Polymer journal* ***2009,*** *41* (9), 752-763.
84. Ramanathan, T.; Fisher, F.; Ruoff, R.; Brinson, L., Amino-functionalized carbon nanotubes for binding to polymers and biological systems. *Chemistry of Materials* ***2005,*** *17* (6), 1290-1295.
85. Damian, C.-M.; Pandele, A. M.; Iovu, H., Ethylenediamine functionalization effect on the thermo-mechanical properties of epoxy nanocomposites reinforced with multiwall carbon nanotubes. *Bull* ***2010,*** *72* (3).
86. Huang, Y.-P.; Lin, I.-J.; Chen, C.-C.; Hsu, Y.-C.; Chang, C.-C.; Lee, M.-J., Delivery of small interfering RNAs in human cervical cancer cells by polyethylenimine-functionalized carbon nanotubes. *Nanoscale research letters* ***2013,*** *8* (1), 1.
87. Kaya, E. N.; Tuncel, S.; Basova, T. V.; Banimuslem, H.; Hassan, A.; Gürek, A. G.; Ahsen, V.; Durmuş, M., Effect of pyrene substitution on the formation and sensor properties of phthalocyanine-single walled carbon nanotube hybrids. *Sensors and Actuators B: Chemical* ***2014,*** *199*, 277-283.
88. Whitaker, C.; Heckert, J. R.; Uber, I. C. *Synthesis of Amide Functionalized Carbon Nanotubes*; DTIC Document: 2007.
89. Kantheti, S.; Gaddam, R. R.; Narayan, R.; Raju, K., Hyperbranched polyol decorated carbon nanotube by click chemistry for functional polyurethane urea hybrid composites. *RSC Advances* ***2014,*** *4* (47), 24420-24427.
90. Qiang, Z.; Liang, G.; Gu, A.; Yuan, L., The interaction between unique hyperbranched polyaniline and carbon nanotubes, and its influence on the dielectric behavior of hyperbranched polyaniline/carbon nanotube/epoxy resin composites. *Journal of Nanoparticle Research* ***2014,*** *16* (5), 1-18.
91. Zardini, H. Z.; Davarpanah, M.; Shanbedi, M.; Amiri, A.; Maghrebi, M.; Ebrahimi, L., Microbial toxicity of ethanolamines—Multiwalled carbon nanotubes. *Journal of Biomedical Materials Research Part A* ***2014,*** *102* (6), 1774-1781.
92. Zhao, Z.; Dai, Y.; Ge, G.; Wang, G., Efficient tuning of microstructure and surface chemistry of nanocarbon catalysts for ethylbenzene direct dehydrogenation. *AIChE Journal* ***2015,*** *61* (8), 2543-2561.
93. Amiri, A.; Zardini, H. Z.; Shanbedi, M.; Maghrebi, M.; Baniadam, M.; Tolueinia, B., Efficient method for functionalization of carbon nanotubes by lysine and improved antimicrobial activity and water-dispersion. *Materials Letters* ***2012,*** *72*, 153-156.

94. Mombeshora, E. T.; Simoyi, R.; Nyamori, V. O.; Ndungu, P. G., Multiwalled carbon nanotube-titania nanocomposites: Understanding nano-structural parameters and functionality in dye-sensitized solar cells. *South African Journal of Chemistry* ***2015,*** *68*, 153-164.
95. Atieh, M. A.; Bakather, O. Y.; Al-Tawbini, B.; Bukhari, A. A.; Abuilaiwi, F. A.; Fettouhi, M. B., Effect of carboxylic functional group functionalized on carbon nanotubes surface on the removal of lead from water. *Bioinorganic chemistry and applications* ***2011,*** *2010*.
96. Yang, K.; Gu, M.; Guo, Y.; Pan, X.; Mu, G., Effects of carbon nanotube functionalization on the mechanical and thermal properties of epoxy composites. *Carbon* ***2009,*** *47* (7), 1723-1737.
97. Kannan, P. K.; Late, D. J.; Morgan, H.; Rout, C. S., Recent developments in 2D layered inorganic nanomaterials for sensing. *Nanoscale* ***2015,*** *7* (32), 13293-13312.
98. Liang, Y.-C.; Liao, W.-K., Annealing induced solid-state structure dependent performance of ultraviolet photodetectors made from binary oxide-based nanocomposites. *RSC Advances* ***2014,*** *4* (37), 19482-19487.